*NAR Cancer*, 2025, **7**, zcaf011
https://doi.org/10.1093/narcan/zcaf011
**DNA Damage Sensing and Repair**

OXFORD

# SRSF2 overexpression induces transcription-/replication-dependent DNA double-strand breaks and interferes with DNA repair pathways to promote lung tumor progression

**Manal Khalife[1,†], Tao Jia[1,2,†], Pierre Caron[1,†], Amani Shreim[1,‡], Aurelie Genoux[1,‡], Agnese Cristini[3], Amelie Pucciarelli[1], Marie Leverve[1], Nina Lepeltier[1], Néstor García-Rodríguez[4], Fabien Dalonneau[1], Shaliny Ramachandran[5], Lara Fernandez Martinez[3], Guillaume Marcion[6], Nicolas Lemaitre[7], Elisabeth Brambilla[7], Carmen Garrido[6], Ester M. Hammond[5], Pablo Huertas[4], Sylvie Gazzeri[1], Olivier Sordet[3], Beatrice Eymin[1,*]**

[1]University Grenoble Alpes, INSERM U1209, CNRS UMR5309, Team RNA Splicing, Cell Signaling and Response to Therapies, Institute for Advanced Biosciences, Grenoble F38000, France
[2]Present address: Key Laboratory of Drug-Targeting and Drug Delivery System of the Education Ministry and Sichuan Province, Sichuan Engineering Laboratory for Plant-Sourced Drug and Sichuan Research Center for Drug Precision Industrial Technology, West China School of Pharmacy, Sichuan University, Chengdu 610041, China
[3]Cancer Research Center of Toulouse (CRCT), INSERM, Université de Toulouse, CNRS, Toulouse 31037, France
[4]Departamento de Genética, Facultad de Biología, Universidad de Sevilla, Sevilla 41080, Spain; Centro Andaluz de Biología Molecular y Medicina Regenerativa (CABIMER), Universidad de Sevilla/CSIC, Sevilla 41092, Spain
[5]Department of Oncology, Oxford Institute for Radiation Oncology, University of Oxford, Oxford OX3 7DQ, United Kingdom
[6]INSERM, UMR1231, Faculty of Medicine and Pharmacy, Université de Bourgogne Franche-Comté, Dijon F21000, France
[7]University Grenoble Alpes, INSERM U1209, CNRS UMR 5309, Team Tumor Molecular Pathology and Biomarkers, Institute for Advanced Biosciences, Grenoble F38000, France

[*]To whom correspondence should be addressed. Tel: +33 4 76 54 94 76; Fax: +33 4 76 54 94 13; Email: Beatrice.Eymin@univ-grenoble-alpes.fr
[†]The first three authors should be regarded as Joint First Authors.
[‡]These authors contributed equally to this paper.

## Abstract

SRSF2 (serine/arginine-rich splicing factor 2) is a critical regulator of pre-messenger RNA splicing, which also plays noncanonical functions in transcription initiation and elongation. Although elevated levels of SRSF2 are associated with advanced stages of lung adenocarcinoma (LUAD), the mechanisms connecting SRSF2 to lung tumor progression remain unknown. We show that SRSF2 overexpression increases global transcription and replicative stress in LUAD cells, which correlates with the production of DNA damage, notably double-strand breaks (DSBs), likely resulting from conflicts between transcription and replication. Moreover, SRSF2 regulates DNA repair pathways by promoting homologous recombination and inhibiting nonhomologous end joining. Mechanistically, SRSF2 interacts with and enhances MRE11 (meiotic recombination 11) recruitment to chromatin, while downregulating 53BP1 messenger RNA and protein levels. Both events are likely contributing to SRSF2-mediated DNA repair process rerouting. Lastly, we show that SRSF2 and MRE11 expression is commonly elevated in LUAD and predicts poor outcome of patients. Altogether, our results identify a mechanism by which SRSF2 overexpression promotes lung cancer progression through a fine control of both DSB production and repair. Finally, we show that SRSF2 knockdown impairs late repair of ionizing radiation-induced DSBs, suggesting a more global function of SRSF2 in DSB repair by homologous recombination.

**Received:** February 24, 2023. **Revised:** February 4, 2025. **Editorial Decision:** March 10, 2025. **Accepted:** March 13, 2025

**Graphical abstract**

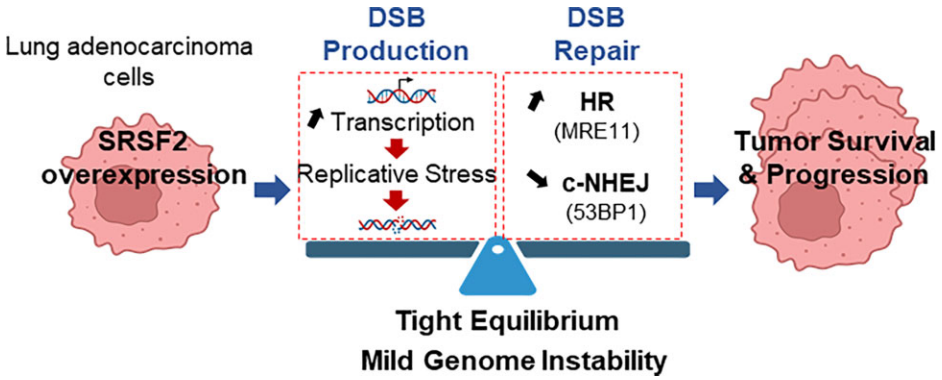


## Introduction

Genome-wide studies have revealed that aberrant pre-messenger RNA (pre-mRNA) splicing, a key post-transcriptional step in the regulation of gene expression [1], is a hallmark of human tumors. Hence, tumor cells express a multitude of cancer-specific splice variants that contribute to all stages of tumorigenesis [2, 3]. In addition, tumor cells exhibit somatic mutations and/or changes (up- or downregulation) in the expression of various components of the spliceosome machinery, including critical splicing factors [4, 5]. However, the molecular mechanisms by which aberrant expression or mutation of splicing regulators contribute to tumorigenesis need to be elucidated further and likely involve both splicing-dependent and/or -independent effects.

DNA double-strand breaks (DSBs) are the most dangerous type of DNA lesions and the main source of genome instability associated with tumorigenesis [6]. In highly proliferative cells, such as cancer cells, conflicts between the replication and transcription machineries are a major cause of DSBs [7, 8], and a source of replication stress that occurs notably in response to overexpression or constitutive activation of oncogenes [9–11]. On one hand, DSBs favor mutations that support cancer progression; on the other hand, DSBs elicit a DNA damage response (DDR) comprising DSB sensing/signaling, cell-cycle checkpoint activation, and DNA repair, which can ultimately lead to apoptosis if repair is not possible [12, 13]. Hence, an accurate management of transcription–replication conflicts (TRCs) and consequently DSBs is required for cancer cell survival. Numerous RNA-binding proteins (RBPs) have been shown to functionally and/or physically interact with DDR components at different levels [14, 15]. For example, RBPs can selectively control the expression of DDR genes [16], assemble at sites of DNA damage together with DNA damage sensors where they participate to DNA repair [17–20], and affect downstream steps of the DDR [21]. Moreover, RBPs hamper the annealing of the nascent RNA to the complementary DNA during transcription, thus preventing the formation of R-loops, structures composed of a RNA:DNA hybrid and a single-stranded DNA, which can be highly mutagenic [22–25]. As a whole, these studies indicate that tight regulation of the RBPs/DDR interplay acts as a barrier against tumorigenesis. It is thus crucial to further address whether and how aberrant expression of RBPs and their mutations in cancer affect the response to DNA damage and promote tumor progression.

The splicing factor SRSF2 (serine/arginine-rich splicing factor 2) belongs to the SR protein family and plays a critical role in the regulation of both constitutive and alternative pre-mRNA splicing [26]. We previously reported the increased expression of SRSF2 in lung tumors, including non-small-cell lung carcinoma (NSCLC) [27] and neuroendocrine lung tumors [28]. In lung adenocarcinoma (LUAD) patients, high levels of SRSF2 protein correlated with advanced clinical stages [27], supporting a role of SRSF2 in lung tumor progression. In this study, we demonstrate that SRSF2 overexpression in LUAD cell lines promotes the accumulation of DSBs, which correlates with a slowdown of replication fork progression, increased global transcription, and R-loop accumulation. Therefore, SRSF2 overexpression might induce conflicts between transcription and replication machineries leading to genomic instability in lung cancer cells. At the molecular level, we further provide evidence of an interplay between SRSF2 and the DNA damage sensor MRE11 (meiotic recombination 11). Moreover, we demonstrate that SRSF2 promotes DSB repair by homologous recombination (HR), which requires MRE11 nuclease activity, whereas it inhibits canonical-nonhomologous end joining (c-NHEJ), which correlates with decreased 53BP1 protein levels. Furthermore, we show that mRNA and protein levels of SRSF2 and MRE11 are positively correlated in NSCLC patients, while the opposite is observed for mRNA levels of *Srsf2* and *53BP1*. In addition, early-stage LUAD patients with high levels of both *Mre11* and *Srsf2* mRNAs exhibit a poorer prognosis. Together, our findings reveal a mechanism underlying the oncogenic function of SRSF2, which involves a regulatory SRSF2/MRE11 cross talk that controls genome stability and cancer cell survival in lung tumors. As we lastly provide evidence that SRSF2 knockdown also impairs late repair of DSBs induced by ionizing radiation (IR), we propose that the function of SRSF2 in DSB repair could extend to various DSB inducers.

## Materials and methods

### Cells, cell culture, and reagents

Human LUAD cell lines (H358, H1299, and A549) were authenticated by DNA Short Tandem Repeat (STR) (ATCC Cell Line Authentification Service, LGC Standards, Molsheim, France) and routinely tested for mycoplasma contamination. Human retinal pigmental epithelial (RPE) *(p53-/-)* cell line was provided by Dr Sylvie Noordermeer (Leiden University Medical Center, LUMC, Oncode Institute, Leiden, The

Netherlands). H358, H1299, and A549 cells were cultured in RPMI-1640 medium/L-GlutaMAX supplemented with 10% (v/v) fetal calf serum (FCS) as previously described [29]. RPE cells were maintained in Dulbecco's modified Eagle's medium GlutaMAX-I (Gibco) with 10% FCS. Generation of stable SRSF2-inducible clones was performed using a modified tetracyclin-regulated inducible expression system (Tet-On System, Clontech). Briefly, H358-Tet-On 4 cells, that stably express the Tet-repressor protein, were co-transfected with pTRE-SRSF2 and pTK-Hyg plasmids using Fugene 6 (Roche Diagnostic, France). Double transfectants cultured in 100 × 20-mm culture dishes were selected for 4 weeks in the presence of hygromycin B (200 μg/ml) and geneticin (G418; 800 μg/ml), and resistant clones were further isolated by successive sub-cultures in 96-, 24-, and 6-well plates. Clones were then screened for SRSF2 induction by western blotting following 24 h of 1-μg/ml doxycyclin treatment. Two clones were arbitrarily selected for further experiments. Other plasmids used in this study were pcDNA3.1-SRSF2-Hemagglutinin (HA) and pcDNA3.1-SRSF2(P95H)-HA encoding HA-tagged SRSF2 wild-type or SRSF2(P95H) mutant protein, pcDNA3.1-MRE11 (a kind gift from Dr MH Gatei, University of Queensland, Australia), pcDNA3.1-NBS1 (a kind gift from Dr JJ Mendiola, The Scripps Research Institute, La Jolla), pGEX-SRSF2(1–60), pGEX-SRSF2(60–115), and pGEX-SRSRF2(115–221) [30]. Transfection of plasmid DNA was performed using XtremeGENE 9 (Roche Diagnostics), Lipofectamine 3000 (Invitrogen), or JetPRIME (Polyplus Transfection, Illkirch, France), according to the manufacturer's instructions. Cells were analyzed between 24 and 48 h after transfection. Cisplatin (cat. #PZ0383, calbiochem), hydroxurea (cat. #H8627), mirin (cat. #M9948), PFM01 (cat. #SML1735), 5,6-dichlorobenzimidazole 1-β-D-ribofuranoside (DRB; cat. #D1916), alpha-amanitin (cat. #A2263), palbociclib (cat. #PZ0383), PHA-767491 (cat. #PZ0178), and roscovitin (cat. #R7772) were from Sigma–Aldrich (Saint Quentin Fallavier, France).

## Generation of stable clones for DNA repair analysis

For these studies, we decided to use the A549 and H1299 LUAD cell lines as they are more efficiently transfectable and express higher level of endogenous SRSF2 protein as compared with H358 cells. For the study of HR, we used the pBL174-pDR-GFP plasmid (a kind gift from Dr Françoise Porteu, INSERM UMR1170, Villejuif). This plasmid contains two inactive genes coding for Green Fluorescent Protein (GFP) under the control of a promoter. The 5′ gene is inactive because of the insertion of a cleavage site for I-SceI. The 3′ gene is inactive because it is deleted in both the 5′ and 3′ directions. When a DSB is produced by I-SceI (e.g. following transient transfection with the I-SceI-encoding pBL133 plasmid), recombination between these two inactive genes restores a functional GFP-coding sequence. To establish stable clones, $10 \times 10^6$ H1299 or A549 cells were transfected with 1 μg pBL174-pDR-GFP plasmid and clones were selected after 5-weeks culture in presence of 5 μg/ml puromycin. In order to select clones efficient for HR, stable clones were transiently transfected with pBL133-SceI plasmid encoding the I-SceI restriction enzyme for 4 days and detection of GFP-positive cells was done by flow cytometry. Four H1299 clones expressing GFP in 1.2%–1.9% of cells as compared with cells transfected with control pcDNA3.1 plasmid were selected for further analyses. Of note, we did not succeed in generating A549-pBL174-pDR-GFP-positive clones. In some experiments, H1299-pBL174 clones were co-transfected for 72 to 96 h with pcDNA3.1-SRSF2-HA plasmid together with pBL133 and treated or not for additional 24 h with 40 μM mirin or 50 μM DRB. Cells were fixed, permeabilized, and incubated with phycoerythrin anti-HA.11 epitope tag antibody (clone 16B12, cat. #901517, Biolegend, United Kingdom). Double HA/GFP-positive cells were quantified by flow cytometry (Accuri C6, BD Biosciences). For RNA interference (siRNA) experiments, stable clones were transfected for 24 h with mismatch (control) or *SRSF2* siRNAs before being transfected with pBL133 for additional 72 h. Percentage of GFP-positive cells was quantified using flow cytometry.

For the analysis of c-NHEJ, we used the pBL230 plasmid (a kind gift from Dr Françoise Porteu, INSERM UMR1170, Villejuif). This plasmid contains genes encoding the membrane antigens CD4 and CD8. CD8 is not expressed as it is in inverted orientation, and CD4 is not expressed because it is too far from the promoter. Two cleavage sites for I-SceI are present in noncoding sequences, which are in direct orientation generating cohesive ends between the two sites. When two DSBs are produced by I-SceI, rejoining of the DNA ends by exclusion or inversion leads to the expression of CD4 or CD8, respectively. Furthermore, $10 \times 10^6$ A549 or H1299 cells were transfected with 1 μg PBL230 plasmid and stable clones were selected after 6-weeks culture in presence of 10 μg/ml blasticidin. Clones having stably integrated PBL230 plasmid were first selected on the basis of the expression of H-2K$^d$, a protein of class I major histocompatibility complex, using flow cytometry after cells fixation in 4% paraformaldehyde (PFA) in 1× phosphate-buffered saline (PBS) and staining using Fluorescein Isothiocyanate (FITC) anti-mouse H-2K$^d$ antibody (clone SF1-1.1, cat. #116605, Biolegend). An irrelevant FITC mouse IgG2a, k isotype was used as a negative control (clone MOPC-173, cat. #400207, Biolegend). Three clones per cell line expressing H-2K$^d$ in >80% cells were selected for further analyses. Detection of efficient c-NHEJ in these selected clones was performed after co-transfection with mismatch (control) or *SRSF2* siRNAs together with PBL133-SceI plasmid for 96 h and detection of CD4 expression by flow cytometry, using an FITC anti-CD4 antibody (clone RM4-5, cat. #553046, BD Biosciences). An irrelevant rat IgG2a, K isotype was used as a negative control (cat. #553929, BD Biosciences). Of note, we did not succeed in detecting CD4 staining in H1299-pBL230 selected clones. Thus, we focused our further studies on A549-pBL230 cells.

## Patients and tissue samples

Seventy-seven human NSCLC patients were included in this study. Tumors consisted of 41 LUAD and 36 squamous lung carcinoma (LUSC). Tumor tissues and normal lung parenchyma, taken away from the bulk of the tumor, were collected from resection of lung tumors, and stored for scientific research in a biological resource repository (Centre de Ressources Biologiques, CHU Grenoble Alpes) following national ethical guidelines. For histological classification, tumor samples were fixed in formalin, and diagnosis was made on paraffin-embedded material using the WHO VIIth classification of lung criteria [31]. For each case, one section from the most representative block was chosen. These sections always contained >70% tumor cells.

## Ethics approval and consent to participate

The study was performed in accordance with the Declaration of Helsinki. All patients enrolled in this study provided written informed consent. Tissue banking and research conduct was approved by the French Ministry of Research (approval AC-2010–1129) and by the regional IRB (CPP 5 Sud Est).

## Generation of DNA damage by IR and immunofluorescence

IR was delivered to RPE, A549, H1299, or H358 cells using an SARRP (Xstrahl SAXO—Grenoble IRMaGe facility) (220 kVp; 13 mA; filtration 0,15 mm Cu; and dose rate 3.057 Gy/min). Cells were analyzed at different timepoints after IR recovery. A549 and H1299 cells were grown on glass coverslips in a 12-well plate, rinsed three times with PBS, and fixed on the coverslips with 10% formalin for 12 min. Next, the cells were rinsed three times with PBS, permeabilized with 0.5% Triton for 5 min, and then rinsed again three times with PBS. Subsequently, 3% PBS–BSA (bovine serum albumin) was added to the cells for 30 min, after which the solution was removed, and a solution of 3% PBS–BSA with γH2AX antibody (clone JBW301, Millipore) was added. After incubation for 2 h or overnight, the cover slips were washed four times with 3% PBS–BSA, and a solution of 3% PBS–BSA with secondary antibody was added. Next, coverslips were placed in the dark. After 2 h, cells were rinsed three times with PBS, and a drop of DAPI-Vectashield (Roche) was placed on a microscope slide, and the coverslip was placed on top of it. Cells were observed using an Olympus microscope (×63 magnification). Images were captured with a Coolview CCD camera (Photonic Science) and digitally saved using Visilog software. The number of γH2A.X foci were analyzed using ImageJ software and the macro Analyze_foci_in_nuclei_fixed_4_61.ijm developed by Bram van den Broek (NKI institute, The Netherlands).

## Clonogenic survival assay

RPE cells were transfected with siRNA (see below), seeded in six-well plates (300 cells per plate) and exposed to different doses of IR. Eight days later, the cells were washed with PBS 1×, fixed with 10% formalin, and stained with methylene blue in borate buffer. Colonies consisting of >50 cells were counted as positive.

## RNA interference

Two sequences designed to specifically target human *SRSF2* RNAs were purchased from Eurogentec (Angers, France) and were as follows: Srsf2_1 5′-UCGAAGUCUCGGUCCCGCACUCG-3′ and Srsf2_2 5′-GCACGAAGGUCCAAGUCCA-3′. In most of the experiments, results obtained with Srsf2_2 siRNA are presented but similar results were obtained with Srsf2_1. A mixture of siRNAs targeting *MRE11* (cat. #sc-37395), *NBS1* (cat. #sc-36061), or *RAD50* (cat. #sc-37397) were purchased from Santa-Cruz (Santa-Cruz Biotechnology, Heidelberg, Germany). For all RNA interference experiments, mismatch (control) siRNA used as a control was 5′-UCGGCUCUUACGCAUUCAA-3′. Cells were transfected with siRNA oligonucleotides duplex using RNAiMAX (Invitrogen, Cergy Pontoise, France) or JetPrime (Polyplus Transfection, Ilkirch, France) reagent according to the manufacturer's instructions. The cells were analyzed 72 h post-transfection.

## RNA extraction and Reverse Transcription quantitative Polymerase Chain Reaction (RT-qPCR) analysis

Total RNA was extracted using NucleoSpin RNA kit (Macherey Nagel) according to the manufacturer's instructions. Total 1 μg RNA was reverse transcribed using iScript™ Reverse Transcription Supermix (Bio-Rad), diluted to 1:10, and 2 μl on 200 μl complementary DNA were used for quantitative PCR (qPCR). The primers were GAPDH-Fw 5′-CGA-GAT-CCC-TCC-AAA-ATC-AA-3′; GAPDH-Rv 5′-ATC-CAC-AGT-CTT-CTG-GGT-GG-3′; TP53BP1-Fw 5′-AAG-CCA-GGC-AAG-AGA-ATG-AGG-C-3′; and TP53BP1-Rv 5′-GGC-TGT-TGA-CTC-TGC-CTG-ATT-G-3′. qPCR was performed using SYBR Green Master Mix (Bio-Rad) according to the manufacturer's instructions on a Bio-Rad CFX96 apparatus. Relative gene expression was calculated, for each sample, as the ratio of specific target gene to GAPDH gene (reference gene), thus normalizing the expression of target gene for sample to sample differences in RNA input.

## Quantification of BrdU incorporation by flow cytometry

Quantification of bromodeoxyuridine (BrdU) incorporation was performed using the APC BrdU Flow kit from BD Pharmingen™ (cat. #sc-552598) according to the manufacturer's instructions. Briefly, $300 \times 10^3$ H358-SRSF2 cells were seeded in six-well plate. After 24 h, 1 μg/ml doxycycline was added or not and cells were cultured for additional 24–48 h. One hour before recovery, cells were incubated with BrdU for 1 h at 37°C, collected, washed in staining buffer, and fixed/permeabilized in BD Cytofix/Cytoperm before staining with anti-BrdU antibody and incubation in 7-aminoactinomycin D (7-AAD) solution. Cells were analyzed by fluorescence-activated cell sorting (FACS, Accuri C6, BD Biosciences or Attune, Invitrogen) using CellQuest (BD Biosciences, Le Pont de Claix, France) or FCS Express 7 Research (Invitrogen, Waltham, USA) softwares.

## Immunofluorescence studies

Immunofluorescence (IF) analyses of S-phase replicating cells were performed using Click-iT EdU (ethynyldeoxyuridine) imaging kit from Invitrogen (Thermo Fisher Scientific, Waltham, USA; cat. #C10340) according to the manufacturer's instructions. Briefly, $3 \times 10^4$ H358-SRSF2 cells were seeded onto 18-mm round coverslips pre-coated with 5 μg/ml fibronectin (cat. #F2006, Sigma–Aldrich), treated or not for 24 h with 1 μg/ml doxycycline, and incubated with 10 μM EdU for 1 h at 37°C. Cells were then fixed with 4% PFA for 15 min at room temperature (RT), permeabilized in 0.5% Triton for 20 min at RT, before performing the Click-iT reaction using Alexa Fluor™ 647 azide. Cells were then stained with anti-γH2AX antibody (clone JBW301, Millipore) for 1 h at RT and nuclei were counterstained using 6-diamidino-2-phenylindole (DAPI). In some experiments, the anti-γH2AX antibody (Cell Signaling, cat. #2577) was also used. Similar protocol for fixation/permeabilization was used for the detection of 53BP1 foci in H358-SRSF2 using anti-53BP1 antibody (Novus, cat. #NB100-304). Cells were observed using

an Olympus microscope (×63 magnification). Images were captured with a Coolview CCD camera (Photonic Science) and digitally saved using Visilog software. Quantification of γH2AX foci number/size/intensity for each condition in each nucleus according or not to EdU-negative or -positive cells was performed using ICY or Image J software. For Rad51 foci detection, H358-SRSF2 cells were plated in poly-lys-coated four-well Lab-Tek II chamber slides, treated or not for 24 h with 1 μg/ml doxycyclin, washed twice with PBS 1×, fixed and permeabilized in ice-cold methanol for 15 min at 4°C, and further permeabilized with 0.5% Triton X-100 for 5 min at RT. After three washes with PBS 1× for 5 min at RT, nonspecific binding sites were blocked with PBS 1×, 10% bovine serum, and 0.3% Triton X-100 for 1 h at RT before overnight incubation at 4°C with anti-Rad51 antibody (Millipore, cat. # PC-130).

For chromatin-bound Replication Protein A (RPA) foci detection, H358-SRSF2 cells were seeded on coverslips, treated or not for 48 h with 1 μg/ml doxycycline, in the presence or not of 40 μM mirin for 24 h or 50 μM DRB for 6 h. Coverslips were then treated for 6 min on ice with pre-extraction buffer [25 mM Tris–HCl (pH 7.5), 50 mM NaCl, 1 mM ethylenediaminetetraacetic acid (EDTA), 3 mM $MgCl_2$, 300 mM sucrose, 0.2% Triton X-100], followed by fixation with 4% paraformaldehyde (w/v) in PBS for 15 min. Then, coverslips were washed twice with PBS and blocked with 5% fetal bovine serum in PBS for 1 h, followed by 2 h incubation with anti-RPA32 antibody (Abcam, cat. #2175). After two washes with PBS, coverslips were incubated with the appropriate secondary antibody for 1 h, washed twice with PBS, and mounted with Vectashield mounting medium containing DAPI (Vector Laboratories). RPA foci were visualized using a Leica Fluorescence microscope equipped with a HCX PL APO 63×/1.4 OIL objective.

## Proximity ligation assay

A549 cells were seeded onto eight-well Lab-Tek II. Proximity ligation assay (PLA) was performed using the Duolink® In Situ kit from Sigma–Aldrich according to the manufacturer's recommendations. In some experiments, cells were cultured or not in the presence of 50 μM cisplatin for 24 h, 50 μM DRB for 6 h, 40 μM mirin or 50 μM PFM101 for 24 h. The antibodies used were rabbit anti-MRE11 (Sigma–Aldrich, cat. # PLA0057), mouse anti-MRE11 (12D7, Genetex, cat. #GTX70212), mouse anti-SRSF2 (Abcam, cat. #ab11826), rabbit anti-γH2AX (Cell Signaling, cat. #2577), or rabbit anti-SRSF2 (Thermo Fisher Scientific, cat. #PA5-12402). Negative controls were performed using rabbit anti-MRE11, rabbit anti-γH2AX, or mouse anti-SRSF2 antibody only, as well as by combining mouse anti-SRSF2 and rabbit anti-HSP90 (C45G5, Cell Signaling, cat. #4877) antibodies. Positive controls were done by detecting either MRE11 or SRSF2 protein using two antibodies from different species. A multiphoton Zeiss (Oberkochen Germany) LSM510 META NLO confocal microscope was used to analyze IF experiments at 63× magnification. Images were acquired with AxioCam digital microscope camera and analyzed using ICY 1.7 software. All images are z-stacked.

## DNA fiber assay

DNA fiber assays were performed as described previously [32]. Briefly, cells were pulse-labeled with chlorodeoxyuridine (CldU; 25 μM) for 20 min, washed once with fresh media, and then followed by the second label iododeoxyuridine (IdU; 250 μM) for 20 min. Fibers were spread, stained and mounted (Invitrogen), and imaged using LSM780 confocal microscope (Carl Zeiss Microscopy Ltd) using a ×63/1.40 Oil DIC M27 Plan-ApoChromat objective.

## Click-iT RNA

In order to detect newly synthesized RNAs, the Click-iT RNA imaging kit (Thermo Fisher Scientific, cat. #C10329) was used according to the manufacturer's instructions. Briefly, $3 \times 10^4$ H358-SRSF2 cells were seeded onto 18-mm round coverslips pre-coated with 5 μg/ml fibronectin and treated or not with 1 μg/ml doxycycline for 24 or 48 h. In some experiments, 50 μM DRB or 10 μg/ml alpha-amanitin was added 6 h before stopping the experiment. Then, cells were incubated for 30 min at 37°C with 1 mM 5-ethynyluridine (EU), fixed with 4% PFA for 30 min at RT, and permeabilized with 0.5% Triton X-100 for 15 min at RT, before performing the Click-iT reaction using Alexa Fluor™ 488 Azide. In some experiments, cells were immunostained with anti-PCNA antibody (PC-10) for 1 h at RT and nuclei were counterstained using Hoechst 33342. Cells were observed using an Olympus microscope (×63 magnification). Images were captured with a Coolview CCD camera (Photonic Science) and digitally saved using Visilog software. Measurement of RNA fluorescence intensity in correlation with or without proliferating cell nuclear antigen (PCNA)-positive or -negative immunostaining was performed for each condition in each nucleus using ICY software.

## RIPA extracts, whole cellular protein extracts, and chromatin-enriched fractions

For RadioImmunoPrecipitation Assay (RIPA) extracts, cells washed three times in 1× PBS were lysed in RIPA buffer [150 mM NaCl, 50 mM Tris–HCl (pH 8.0), 0.1% sodium dodecyl sulfate (SDS), 1% Nonidet P40, 0.5% sodium deoxycholate, 0.1 mM phenylmethanesulfonyl fluoride (PMSF), 2.5 μg/ml pepstatin, 10 μg/ml aprotinin, 5 μg/ml leupeptin, 0.2 mM $Na_3VO_4$] for 30 min on ice and pelleted by centrifugation at 13 200 rpm for 20 min at 4°C. For whole cellular protein extracts (WCEs), cells were lysed in denaturing buffer [20 mM Tris–HCI (pH 7.5), 50 mM NaCI, 0.5% IGEPAL, 1% sodium deoxycholate, 1% SDS, 5 mM $MgCl_2$, protease inhibitor cocktail (Roche)]. Chromatin-enriched fractions were prepared according to a previously described protocol [33]. Briefly, $2 \times 10^6$ cells were incubated for 10 min on ice in a hypotonic buffer [10 mM HEPES (pH 7.9), 1.5 mM MgCl2, 12% sucrose, 10% glycerol, 1 mM DTT supplemented just before use with phosphatases, proteases inhibitors] and centrifuged for 4 min at 1300 × *g*. Supernatants (fraction S1) were eliminated and cell nuclei were incubated for 10 min on ice in a buffer containing 3 mM EDTA, 0.2 mM EGTA, and 1 mM DTT with phosphatases and proteases inhibitors before centrifugation at 1700 × *g* for 4 min. Supernatant (fraction S2 containing soluble nuclear proteins) was eliminated and cell pellet containing nuclear proteins tightly bound to chromatin (P2 extracts, chromatin-enriched fractions) was resuspended in Laemmli 1× [0.125 M Tris–HCl (pH 6.8), 2% SDS, 10% glycerol, 5% 2-mercaptoethanol, 0.002% bromophenol blue] and sonicated. Proteins were quantified and 20–40 μg proteins were separated by sodium dodecyl sulfate–polyacrylamide gel electrophoresis (SDS–PAGE) for 3 h at

75 V using 4%–12% precast polyacrylamide gels (Invitrogen) and 20× 3-morpholinopropane-1-sulfonic acid (MOPS) running buffer (Invitrogen). Next, proteins were transferred onto polyvinylidene difluoride (PVDF) membranes (Promega) for 2 h at 52 V. The membrane was probed with primary antibodies (Supplementary Table S1) for 2 h or overnight and washed three times with 0.1% PBS-Tween-20 followed by incubation with secondary antibodies for 2 h. Membranes were scanned and analyzed using Fusion camera (Vilber).

## Immunoprecipitation

For immunoprecipitation, A549 cells were transiently transfected for 24 h with pcDNA3.1, pcDNA3.1-SRSF2-HA, or pcDNA3.1-SRSF2(P95H)-HA plasmid. Cells were then lysed on ice using RIPA buffer supplemented with proteases and phosphatases inhibitors. Briefly, 500 μg to 1 mg of total protein extracts were pre-cleared for 1 h in presence of protein G-magnetic beads (Surebeads™, Bio-Rad), then incubated with protein G beads and anti-HA antibody (clone 3F10, Roche Diagnostics) overnight at 4°C. An irrelevant rat IgG1 isotype was used as control for immunoprecipitation.

## Isolation of proteins on nascent DNA

In order to detect proteins that localize at replication forks, isolation of proteins on nascent DNA (iPOND) was performed as described in [34]. Briefly, 25 × $10^6$ H358-SRSF2 cells treated or not for 24 h with 1 μg/ml doxycycline were incubated with 10 μM EdU for 13–18 min at 37°C, then 1% formaldehyde was added to cross-link proteins to DNA for 20 min at RT and quenching of cross-link reaction was done by adding 1.25 M glycine. Cells were permeabilized in 0.25% Triton X-100 for 30 min at RT before performing the click chemistry reaction to conjugate biotin to EdU. In all experiments, a negative control without biotin azide was added as a no click reaction. Cells were then lysed in 50 mM Tris–HCl (pH 8.0), 1% SDS supplemented just before use with protease inhibitors, sonicated, and DNA–protein complexes were captured by adding streptavidin magnetic beads and incubating 16 h in cold room while rotating. In each condition, a fraction of lysate was saved before adding streptavidin-agarose beads as an input sample. After extensive bead washes, protein–DNA cross-links were reversed and proteins were denatured by adding 1:1 (v/v) of packed beads SDS sample buffer 2× for 25 min at 95°C before separation on SDS–PAGE gel. PCNA and RPA70 proteins present at replication forks were detected by immunoblotting. Histone H3 was used as a control.

## Neutral comet assay

Neutral comet assays were performed according to the manufacturer's instructions (Trevigen), except that electrophoresis was performed at 4°C. Slides were scanned by using a AxioObserver Z1 fluorescence microscope (Zeiss) with the objective EC Plan-Neofluar 10×/0.3 Ph1. Comet tail moments were measured with ImageJ software (version 1.51n) with the plugin OpenComet (http://opencomet.org/).

## RNA/DNA hybrid slot blot

Slot blot experiments were performed as previously described [35, 36]. Briefly, non-cross-linked nuclei were isolated by lysing cells [85 mM KCl, 5 mM Pipes (pH 8.0), 0.5% NP-40] and then, subjected to nuclear lysis [50 mM Tris–HCl (pH 8.0), 5 mM EDTA, 1% SDS]. Lysates were digested with proteinase K (#3115828001; Sigma–Aldrich) at 55°C for 3 h and genomic nucleic acids were precipitated with isopropanol followed by a wash in 75% ethanol. Where relevant, samples were treated with 1.7 U of RNase H (#M0297; NEB) per microgram of genomic DNA for 3.5 h at 37°C. Genomic nucleic acids were spotted into a Hybond™-$N^+$ membrane and ultraviolet-cross-linked. The membrane was saturated and probed with S9.6 antibody (#MABE1095, Merck-Millipore) to detect RNA/DNA hybrids and an anti-dsDNA antibody (#ab27156; Abcam) to detect double-stranded DNA (dsDNA), used as a loading control. Decreasing concentrations of genomic nucleic acids were probed with the S9.6 antibody (1 and 0.5 μg) and the anti-dsDNA antibody (30 and 15 ng). Images were acquired with a ChemiDoc MP Imaging System (Bio-Rad) and signals quantified using ImageLab software (version 6.0.1).

## Biolayer interferometry

*In vitro* transcribed/translated recombinant SRSF2-HA and SRSF2(P95H)-HA proteins were produced using TNT® coupled wheat germ extracts system (Promega, Charbonnières les Bains, France), according to the manufacturer's instructions. Empty pcDNA3.1 plasmid was used as a negative control. MRE11A recombinant protein (H00004361-P01) was from Abnova (Novus Biologicals, United Kingdom). The interaction between MRE11 and SRSF2 or SRSF2(P95H) mutant was assessed by biolayer interferometry with an Octet Red instrument as previously described [37, 38]. Biosensors coated with anti-GST antibody were used to load GST-conjugated MRE11 (10 μg/ml) in kinetic buffer (KB). Hence, binding with SRSF2 and SRSF2-P95H produced using TNT-coupled wheat germ extracts were performed by dipping MRE11-coated biosensor in 4 times diluted lysates in KB for 300 s. Then, the dissociation was measured by transferring the biosensors in KB for 600 s.

## Immunohistochemistry on patient samples

Immunohistochemical (IHC) analysis was carried-out on formalin- or paraffin-embedded tissue sections as previously described [27]. Antibody for MRE11 immunostaining was mouse monoclonal anti-MRE11 (clone 12D7, cat. #GTX70212, Euromedex, Soufflenweyersheim, France). For immunostaining evaluation, a score (0–300) was established by multiplying the percentage of labelled cells (0%–100%) by the staining intensity (0, null; 1, low; 2, moderate; 3, strong). Scores obtained for alveolar type II pneumocytes and bronchial cells in normal lung tissues taken at distance from the tumor were considered as normal scores for LUAD and LUSC, respectively. SRSF2 IHC scores were retrieved from our previous work [27].

## Data mining of publicly available databases and statistical analyses

Expression values for *Srsf2*, *53BP1*, and *Mre11* mRNAs were retrieved from human tumors and matched healthy tissues collected by Genomic Data Commons TCGA Lung Adenocarcinoma (TCGA LUAD). They were downloaded as log2 (FPKM-UQ + 1) values using UCSC Xena platform [39]. Another three LUAD Gene Expression Omnibus datasets, namely GSE434582 [40], GSE68465 [41], and GSE720943 [42], were used to perform confirmative study of expression of *Srsf2*

and *Mre11* mRNAs. The clinical annotations of LUAD patients, including pathological stages and survival time, were obtained from UCSC Xena platform. The expression data as RNA normalized log2 transformed value and patient's phenotypical information were retrieved using the online tool of GEO2R [43] and the GEOquery and limma R packages from the Bioconductor project. The correlation analysis between *Srsf2* and *Mre11* mRNAs expression values in primary LUAD patients group and matched normal tissue group was calculated by Spearman's correlation coefficients and statistical significance using GraphPad Prism 8 software. For Kaplan-Meier (KM) studies, all pTNM stages, I/II stages or stage I patients were sub-divided in two classes (high expression, low expression) according to *Srsf2* mRNA median value. In each group, patients were then sub-divided in two classes according to *Mre11* mRNA levels (high expression: >75th percentile, 4th quartile; low-middle expression: <75th percentile, 1st–3rd quartiles). Univariate survival analyses were done using the Kaplan–Meier method and *P*-values were derived from a log-rank test. Overall survival was calculated from the date of surgery to the date of death. *P*-values $< 0.05$ were considered significant. Descriptive analyses comparing continuous and two-level categorical variables were carried out using the Mann–Whitney *U*-test. All statistical analyses were performed using GraphPad Prism 8.0 software.

## Results

### SRSF2 overexpression induces DSBs in LUAD cells

To investigate how SRSF2 contributes to lung tumor progression, we generated H358 LUAD cells inducible for SRSF2. H358 cells express lower level of endogenous SRSF2 compared with other LUAD cells, such as H1299 and A549 cells. Immunoblotting experiments showed that SRSF2 overexpression increased γH2AX (phosphorylated H2AX on Ser139) and pATM (phosphorylated ATM on Ser1981), a kinase that phosphorylates H2AX (Fig. 1A and B and Supplementary Fig. S1A). γH2AX accumulation after 48 h of SRSF2 induction was similar to that observed after 24 h of treatment with hydroxyurea (HU), a replicative stress inducer (Fig. 1B). Increased number and area of γH2AX foci per nucleus were also detected by IF microscopy in SRSF2-overexpressing H358 cells (Fig. 1C), and neutral comet assay provided direct evidence for the presence of DSBs (Fig. 1D). This suggested that γH2AX accumulation likely reflects increase of DSBs, although H2AX can also be phosphorylated in response to other types of DNA damage [44]. PLA experiments further showed closed proximity between endogenous SRSF2 and γH2AX proteins in A549 LUAD cells (Fig. 1E), suggesting that SRSF2 is also present at endogenous DSB sites in lung tumor cells. Interestingly, the number of SRSF2/γH2AX PLA foci increased in response to cisplatin treatment, a genotoxic chemotherapy that also leads to replicative stress and DSBs (Fig. 1F). Of note, no PLA interactions were detected between SRSF2 and HSP90 used as an irrelevant negative control protein (not shown). Altogether, these results indicate that SRSF2 overexpression induces DSBs and DDR activation in lung cancer cells.

### SRSF2-induced DSBs are associated with replicative stress

Analysis of cell cycle distribution by two-dimensional flow cytometry after co-staining with BrdU and 7-AAD-A showed a slight but reproducible increase in the percentage of cells in G2/M upon SRSF2 overexpression, which started after 24 h of induction (Fig. 2A and Supplementary Fig. S1B). In addition, SRSF2 overexpression decreased the percentage of cells incorporating BrdU in S phase (Fig. 2A and Supplementary Fig. S1B), suggesting the occurrence of replicative stress [45]. To test this possibility, we analyzed the length of replication forks by a DNA fiber assay (Fig. 2B). Replication fork progression was assessed by sequential incorporation of CldU and IdU. CldU- and IdU-positive DNA fibers were then visualized by microscopy (Fig. 2B, upper panels) and CldU and IdU track lengths were measured only on double-labeled forks to evaluate the speed of ongoing replication forks (Fig. 2B, lower panels). SRSF2-overexpressing cells showed shorter IdU-labeled track lengths, indicating slowing of replication fork progression (Fig. 2B, lower panel). To investigate further, we performed iPOND experiments to analyze proteins at nascent replication forks [34]. In agreement with replicative stress [46], SRSF2 overexpression decreased the amount of the DNA polymerase processivity factor PCNA at replication forks in H358 cells, while RPA70 recruitment, a marker of ssDNA, increased (Fig. 2C), which could be consistent with stalled replication forks. From these results, we conclude that SRSF2 overexpression in LUAD cells slows-down replication fork progression, thereby indicating enhanced replicative stress.

Therefore, to test whether SRSF2-induced DSBs could depend on replicative stress, we combined γH2AX immunostaining with Click-iT-EdU assay to analyze γH2AX in S phase (EdU-positive) and non-S phase (EdU-negative) cells by IF microscopy. As compared with control cells, SRSF2 overexpression in H358 cells increased γH2AX in EdU-positive cells, while no significant increase was observed in EdU-negative cells (Fig. 2D). These results suggest that SRSF2 overexpression triggers replication-dependent DSBs. To further assess the role of replication on SRSF2-induced DSBs, we tested the effect of palbociclib, a CDK4/CDK6 inhibitor, which prevents S-phase entry [47]. Palbociclib reduced the accumulation of γH2AX protein upon SRSF2 overexpression (Fig. 2E). Similar results were obtained with two broad CDK inhibitors, PHA-767491 and roscovitin, which block both replication and transcription (Fig. 2F). Together, these results show that SRSF2 overexpression induces DSBs that occur mainly in replicative cells.

### SRSF2-induced DSBs depend on transcription

Besides its function in RNA splicing, SRSF2 has been implicated in promoting transcription initiation and elongation [48–51]. Increased transcription can cause TRCs and DNA damage [52–54]. Therefore, we investigated whether SRSF2-induced replication-dependent DSBs (Fig. 2) could also depend on increased transcription. First, we analyzed global transcription activity by measuring the incorporation of EU in nascent RNA by IF microscopy. Transcription was increased in SRSF2-overexpressing cells after 48 h (Fig. 3A) or 24 h (Fig. 3B) induction. EU/PCNA co-immunostaining showed that elevated transcription upon SRSF2 overexpression was detected in both S and non-S phase cells (Fig. 3B). We also noticed that, among SRSF2-overexpressing cells, PCNA-positive cells (S phase cells) exhibited higher transcription compared with PCNA-negative cells (Fig. 3B). Together with the observations that SRSF2 overexpression slows-down replication fork progression (Fig. 2B) and induces γH2AX

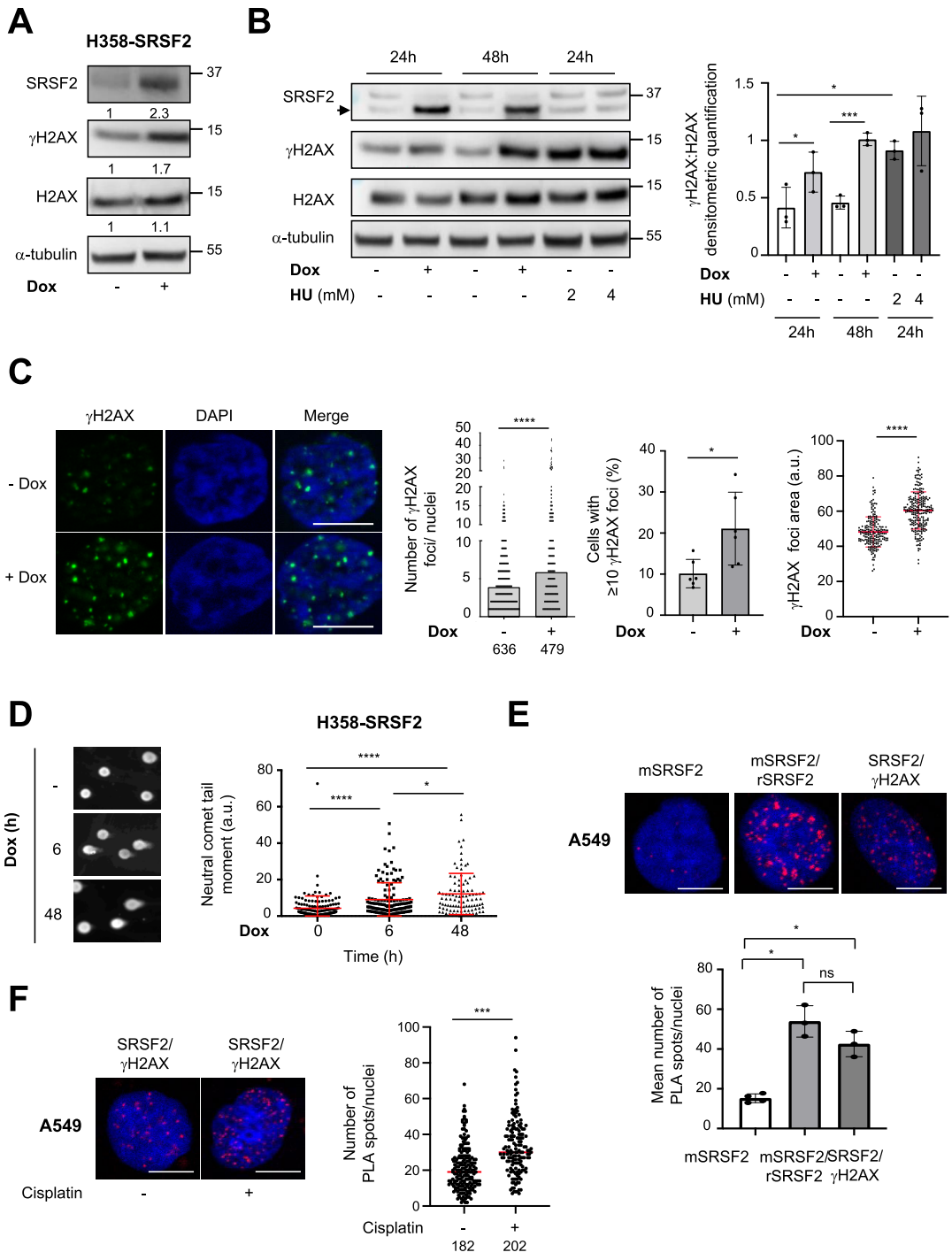


**Figure 1.** SRSF2 overexpression induces DSBs. (A–D) H358-SRSF2-inducible cells were cultured (+) or not (−) with doxycycline (Dox) (1 μg/ml) for 24 h (A, C) or for the indicated times (B, D). In some experiments, H358-SRSF2 cells were cultured in presence of HU (2 or 4 mM) for 24 h. (**A**) Representative immunoblots of indicated proteins. $n = 3$. Numbers represent densitometric quantification of specific protein signal normalized to α-tubulin signal. (**B**) Left panel: Representative immunoblots of indicated proteins. Right panel: Densitometric quantification (mean ± SD) of the γH2AX:H2AX ratio normalized to α-tubulin signal. $n = 3$. Paired *t*-test. $^{*}P < .05$, $^{***}P < .001$. (**C**) Left panel: Representative immunostainings of γH2AX foci. DAPI was used to counterstain the nucleus. Scale bar = 10 μm. Middle panels: Quantification of γH2AX foci number/nucleus and percentage of cells with ≥10 foci/nucleus (mean ± SD). Right panel: γH2AX foci area/nucleus (mean ± SD). $n = 2$ biological replicates performed in triplicate. Unpaired *t*-test, $^{*}P < .05$, $^{****}P < .0001$. (**D**) Detection of DSBs by neutral comet assay. Left panel: Representative pictures of nuclei. Right panel: Quantification of neutral comet tail moments. Mean ± SD. $n = 3$. Unpaired *t*-test, $^{****}P < .0001$, $^{*}P < .05$. (**E**) Upper panel: PLA for the detection of the closed proximity between endogenous SRSF2 and γH2AX proteins in A549 cells. mSRSF2: PLA with mouse anti-SRSF2 antibody only as a negative control. mSRSF2/rSRSF2: PLA with mouse and rabbit anti-SRSF2 antibodies as a positive control. SRSF2/γH2AX: PLA with mouse anti-SRSF2 and rabbit anti-γH2AX antibodies. Scale bar = 10 μm. Lower panel: Quantification of SRSF2 and γH2AX PLA interactions/nucleus from four (mSRSF2) or three (mSRSF2/rSRSF2; SRSF2/γH2AX) independent experiments ($n = 50$–$60$ cells/condition). Mean ± SD. Unpaired *t*-test, $^{*}P < .05$, ns: not significant. (**F**) SRSF2 and γH2AX PLA interactions in A549 cells treated (+) or not (−) with 50 μM cisplatin for 24 h. Left panel: Representative images. Scale bar = 10 μm. Right panel: Quantification of the number of PLA interactions/nucleus. Mean is indicated. $n = 2$. Unpaired *t*-test. $^{***}P < .01$. In all immunoblot data, α-tubulin was used as a loading control.

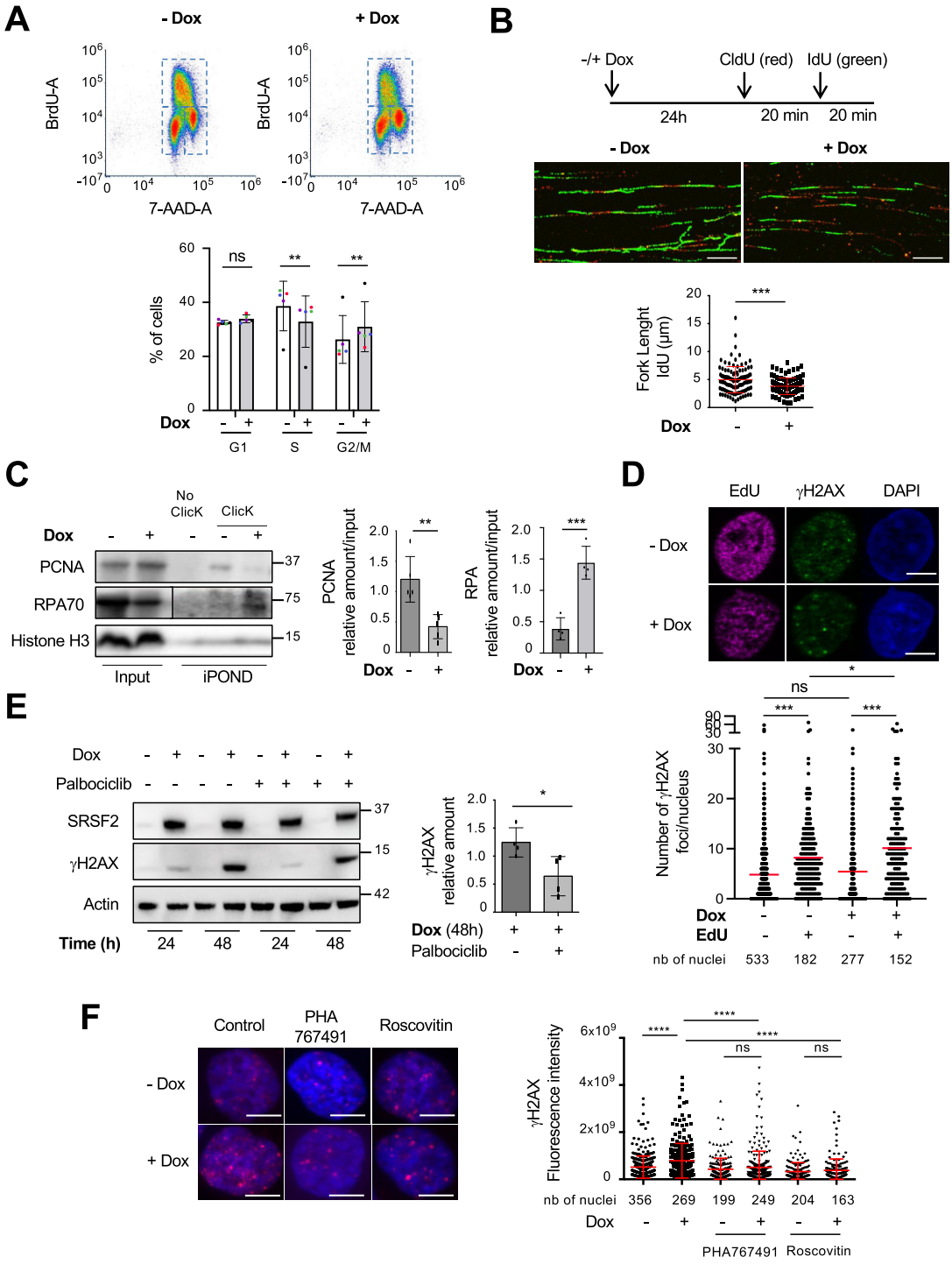


**Figure 2.** SRSF2 overexpression induces replication-dependent DSBs. H358-SRSF2 cells were cultured with (+) or without (−) doxycycline (Dox) (1 μg/ml) for 24 h (A–F) or 48 h (E). (**A**) Upper panels: Representative experiment of FACS analysis of BrdU- and 7-AAD-A-positive cells. Lower panel: Quantification of the cell cycle distribution (%). Mean ± SD, $n = 5$. Paired *t*-test, $^{**}P < .01$, ns: not significant. (**B**) H358-SRSF2 cells were sequentially labelled with CldU and IdU and DNA fibers were prepared. CldU and IdU were detected using specific antibodies. Upper panels: Representative IF images showing CldU- and IdU-positive tracks. Scale bar = 5 μm. Lower panel: Lengths (μm) of IdU-positive replication tracks in control cells (−Dox, $n = 107$) and SRSF2-overexpressing cells (+Dox, $n = 101$). Mean ± SD. Mann–Whitney *t*-test, $^{***}P < .001$. (**C**) iPOND experiment for the detection of PCNA or RPA70 protein at nascent replication forks by immunoblotting. Left panel: Representative immunoblots. Histone H3 was used as a control of equal DNA amount. No click: Negative control. Right panels: Densitometric quantification of PCNA and RPA70 normalized to input. Mean ± SD. *t*-test, $^{**}P < .01$, $^{***}P < .001$. (**D**) Upper panel: Representative images of IF staining of EdU and γH2AX. DAPI was used to counterstain the nucleus. Scale bar = 10 μm. Lower panel: Quantification of γH2AX foci number/nucleus in EdU-positive or -negative cells. Mean. $n = 3$. Unpaired *t*-test, $^{*}P < .05$, $^{***}P < .001$, ns: not significant. (**E**) Representative immunoblots of SRSF2 and γH2AX in H358-SRSF2 cells cultured with or without palbociclib (2 μM) for the indicated times. Actin was used as a loading control. Right panel: Quantification (mean ± SD) of γH2AX level. $n = 4$. Mann–Whitney *t*-test, $^{*}P < .05$. (**F**) Left panel: Immunostaining of γH2AX in H358-SRSF2 cells cultured with or without doxycycline (1 μg/ml) for 24 h in the presence or absence (control) of PHA767491 or roscovitin (10 μM each) for 2 h before staining. DAPI was used to counterstain nuclei. Scale bar = 10 μm. Right panel: Distribution of γH2AX (mean ± SD) fluorescence intensity in each condition. $n = 3$. Mann–Whitney *t*-test, $^{****}P < .0001$, ns: not significant.

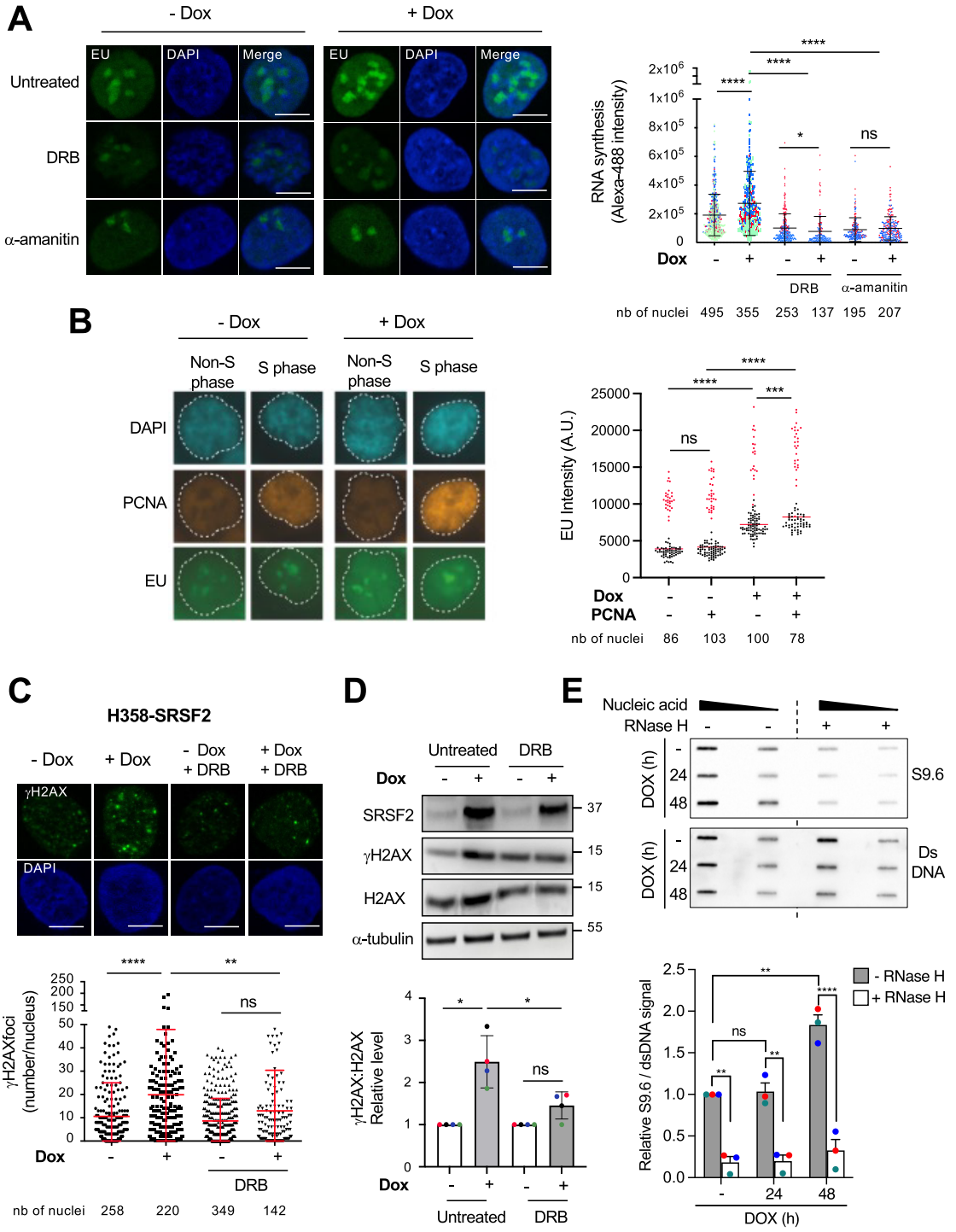


**Figure 3.** SRSF2-induced DSBs depend on transcription. (A–E) H358-SRSF2 cells were cultured in the presence (+Dox) or absence (−Dox) of doxycycline (1 μg/ml). (**A**) Click-iT RNA assay in which EU incorporation was used to detect nascent RNA synthesis. DRB (50 μM) or α-amanitin (10 μg/ml) was added for 6 h following 42-h doxycycline treatment. Left panels: Representative images of EU staining. DAPI was used to counterstain the nucleus. Scale bar = 10 μm. Right panel: Quantification of Alexa-488 intensity/nucleus. Mean ± SD. $n = 3$ for dox−/dox+ conditions and $n = 2$ for DRB/α-amanitin conditions. Mann–Whitney *t*-test, $^{*}P < .05$, $^{****}P < .0001$, ns: not significant. (**B**) Click-iT RNA combined with PCNA immunostaining to detect cells in non-S phase and S phase and cultured or not with doxycycline (1 μg/ml) for 24 h. Left panels: Representative images of EU and PCNA stainings. DAPI was used to counterstain the nucleus. Right panel: Quantification of EU intensity/nucleus in nucleoplasm only (excluding nucleoli staining). Median of two independent experiments (color coded). Mann–Whitney *t*-test. $^{***}P < .001$, $^{****}P < .0001$, ns: not significant. (C, D) DRB was added or not for 6 h following 18-h doxycycline treatment. (**C**) Upper panels: Representative illustrations of γH2AX immunofluorescent staining. DAPI was used to counterstain nuclei. Scale bar = 10 μm. Lower panel: Number of γH2AX foci/nucleus. $n = 3$. Mann–Whitney *t*-test, $^{****}P < .0001$, $^{**}P < .01$, ns: not significant. (**D**) Upper panel: Representative immunoblots of indicated proteins. α-Tubulin was used as a loading control. Lower panel: Relative γH2AX:E2AX ratio according to α-tubulin signal. Ratio obtained in non-induced conditions was arbitrarily assigned the value 1. Mean ± SD. $n = 4$. Paired *t*-test, $^{*}P < .05$, ns: not significant. (**E**) RNA/DNA hybrid slot blot of genomic DNA ± RNAse H from H358-SRSF2 cells cultured with doxycycline (DOX) for the indicated times. Upper panel: Representative slot blot. dsDNA: Loading control. Lower panel: Values are normalized to dsDNA (means ± SEM; $n = 3$). Two-tailed unpaired *t*-test, $^{****}P < .0001$, $^{**}P < .01$, ns: not significant.

accumulation mainly in EdU-positive cells (Fig. 2D), these results suggest that SRSF2 overexpression leads to TRCs, which contribute to DSB formation. Therefore, to test whether transcription is involved in SRSF2-induced DSBs, we used the transcription inhibitor DRB, which efficiently prevented SRSF2-induced transcription (Fig. 3A). DRB was also found to inhibit SRSF2-induced γH2AX accumulation, assessed by IF (Fig. 3C) and immunoblotting (Fig. 3D). Therefore, ongoing transcription appears required for SRSF2-induced DSBs. Taken together, these results indicate that SRSF2-induced DSBs likely result from conflicts between replication and transcription machineries.

Noteworthy, it has been shown that R-loop accumulation is favored by increased RNA synthesis [52, 55]. In addition, multiple studies have now identified abnormal accumulation of R-loops as a shared molecular consequence downstream of spliceosome gene mutations [56, 57] or inactivation [23]. Therefore, we tested the impact of SRSF2 overexpression on R-loop formation. We detected R-loops in SRSF2-overexpressing cells that started to accumulate after 48 h induction (Fig. 3E). This suggests that increases in DNA damage, transcription, and replicative stress, which are already detected after 24 h SRSF2 induction (Figs 1, 2B, and 3B), somewhat precede R-loop appearance in our cellular model.

## SRSF2 interacts with and regulates the recruitment of MRE11 to chromatin

Besides demonstrating that SRFS2 overexpression induces replication-/transcription-dependent DSBs leading to γH2AX accumulation, we also found that SRSF2 lies in closed proximity with γH2AX (Fig. 1E and F). These results led us to investigate further the interplay between SRSF2 and some components of the DDR machinery present at DSB sites. The MRE11/RAD50/NBS1 (MRN) complex is one of the first sensors and responders to DSBs. It orchestrates DDR response by contributing notably to the activation of ATM kinase, which in turn phosphorylates H2AX [58, 59]. Therefore, we first analyzed the impact of SRSF2 on the expression and recruitment of MRN to chromatin. In H358 cells, SRSF2 overexpression slightly decreased the expression of NBS1 (Fig. 4A), while it increased the levels of MRE11 to chromatin (Fig. 4B). Conversely, SRSF2 depletion upon siRNA decreased MRE11 recruitment to chromatin without affecting its expression level in whole-cellular extracts from both A549 and H1299 LUAD cells (Fig. 4C). Then, we tested whether SRSF2 could bind to the MRN complex. A549 LUAD cells were transiently transfected with a plasmid encoding HA-tagged wild-type SRSF2 and co-immunoprecipitation (co-IP) was carried out with an anti-HA antibody. SRSF2 co-IP contained the three components of the MRN complex (Fig. 4D), indicating that at least a fraction of overexpressed SRSF2 is interacting with MRE11, RAD50, and NBS1 proteins. To further assess whether SRSF2 and MRE11 could interact directly, we performed a biolayer interferometry experiment using recombinant MRE11 as bait and *in vitro* transcribed-translated SRSF2. In this assay, we observed a rapid interaction between MRE11 and SRSF2 recombinant proteins as compared with negative pcDNA3 lysate (Fig. 4E). These results suggest that MRE11 and SRSF2 proteins can directly interact, although we cannot exclude that the interaction is weak as we did not compare SRSF2/MRE11 binding with that of RAD50/MRE11 for instance. Therefore, to go further, we also performed GST pull-down assays by incubating recombinant GST-SRSF2(1–60), GST-SRSF2(60–115), or GST-SRSF2(115–221) recombinant proteins (Supplementary Fig. S2A) with either cellular lysates from H358 cells (Supplementary Fig. S2B) or *in vitro* transcribed-translated MRE11 or NBS1 protein (Supplementary Fig. S2C). As compared with control GST protein or other GST-SRSF2 fragments, we observed that GST-SRSF2(115–221), which encompasses the Arginine/Serine-Rich (RS) domain of SRSF2 involved in protein–protein interactions, pulled down endogenous and recombinant MRE11 but not NBS1 protein. In addition, we showed a closed proximity between endogenous SRSF2 and MRE11 proteins by performing PLA in A549 cells (Fig. 4F) and in H358-derived xenografts in nude mice (Supplementary Fig. S3). Altogether, these results indicate that SRSF2 can interact with and enhance the recruitment of MRE11 to chromatin. Interestingly, the number of SRSF2/MRE11 PLA foci increased in A549 cells treated with cisplatin (Supplementary Fig. S4), which further supports a role of the SRSF2/MRE11 cross talk in response to replicative stress inducers.

We also tested whether the cancer-associated SRSF2 mutant, referred to as SRSF2(P95H) [60, 61], is able to interact with MRE11. This mutant has been previously linked to replicative stress, R-loop formation, and genome instability in haematological malignancies [60]. As compared with SRSF2, SRSF2(P95H) did not co-IP with the MRN complex (Fig. 4D) and biolayer interferometry experiments did not show a strong interaction between MRE11 and SRSF2(P95H) (Fig. 4E). In addition, and in line with a possible role of the SRSF2/MRE11 interaction in MRN recruitment to chromatin, SRSF2(P95H) did not promote accumulation of MRE11 to chromatin as compared with wild-type SRSF2, although it was present in chromatin-enriched fraction to the same extent than wild-type SRSF2 (Fig. 4G).

MRE11 exhibits both an exonuclease and an endonuclease activity, as well as nuclease-independent functions (e.g. DNA tethering) [62, 63]. To investigate whether the nuclease activity of MRE11 is required for its interaction with SRSF2, we used mirin or PFM101 to preferentially inhibit MRE11 exonuclease or endonuclease activity, respectively [64, 65]. Neither inhibitor prevented the PLA interactions between endogenous SRSF2 and MRE11 in A549 cells (Supplementary Fig. S5), suggesting that the binding of SRSF2 to MRE11 is independent of MRE11 nuclease activity. Because we showed that SRSF2 promotes transcription-dependent DSBs (Fig. 3), we also tested whether endogenous SRSF2/MRE11 interaction could depend on transcription. Remarkably, the inhibition of transcription with DRB significantly decreased the number of SRSF2/MRE11 PLA foci in A549 cells (Fig. 4H). Taken together, these results provide evidence of a direct cross talk between SRSF2 and MRE11 proteins in LUAD cancer cells, which requires active transcription and correlates with enhanced recruitment of MRE11 to chromatin in SRSF2-overexpressing cells.

## SRSF2 promotes DNA repair by HR and inhibits c-NHEJ

To assess the functional relevance of SRSF2-dependent recruitment of MRN to chromatin, we depleted MRN components in SRSF2-overexpressing H358 cells. We observed that siRNA-mediated depletion of MRE11, RAD50, or NBS1 led to an increase in γH2AX and active caspase-3 (Fig. 5A),

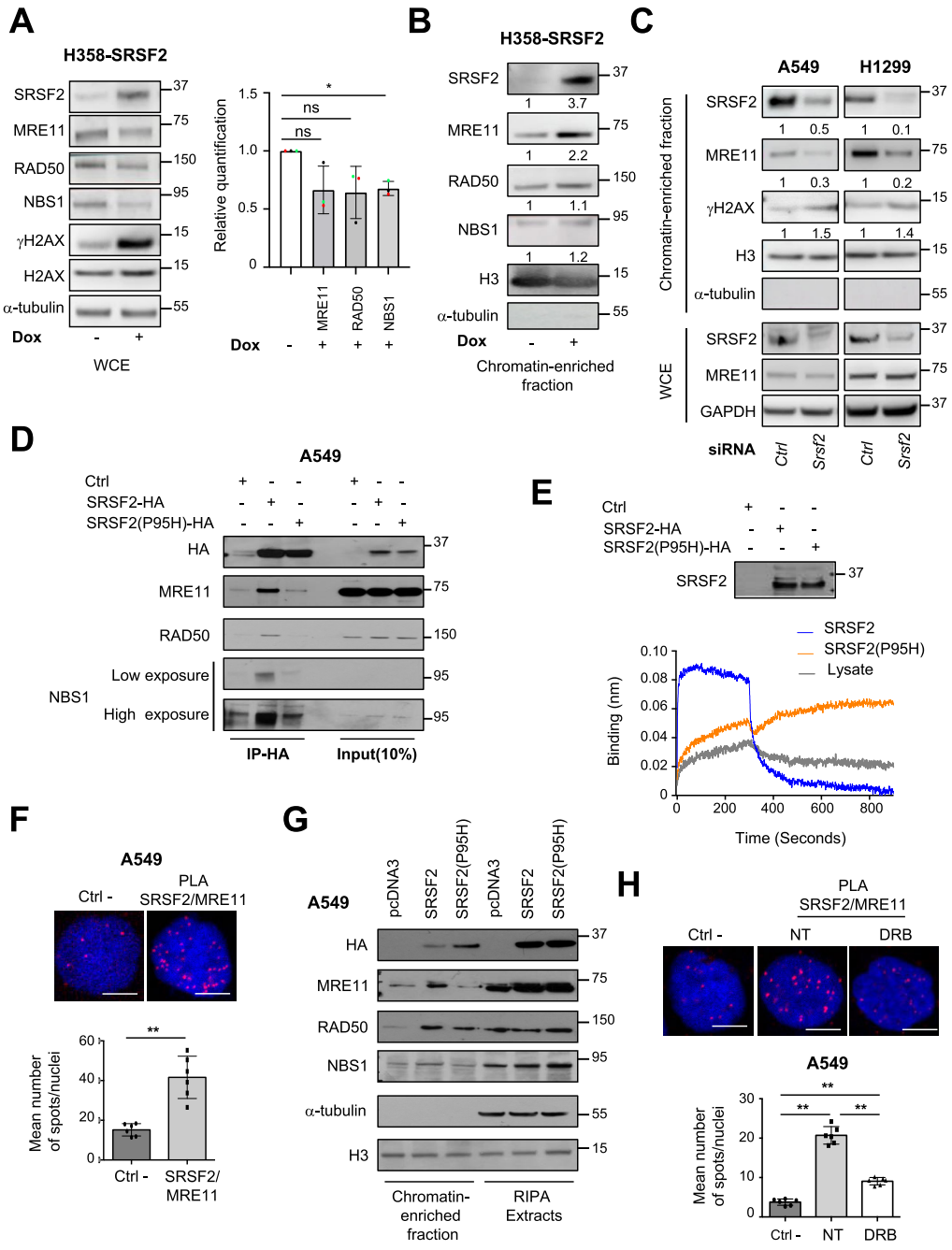


**Figure 4.** SRSF2 interacts with and increases MRE11 recruitment to chromatin. (A, B) Representative immunoblots of indicated proteins in WCEs (A, left panel) or chromatin-enriched fractions (B) from H358-SRSF2 cells cultured in the presence (+) or absence (−) of doxycycline (1 μg/ml) for 48 h. (**A**) Right panel: Relative quantification of MRE11/RAD50/NBS1 protein level normalized to α-tubulin. Ratio in uninduced condition was arbitrarily assigned the value 1. Mean ± SD. $n = 3$. Paired *t*-test, $^{*}P < .05$, ns: not significant. (**B**) A representative experiment out of three is illustrated. Numbers represent the quantification of densitometric signals according to histone H3 signal. (**C**) Representative immunoblots of indicated proteins in A549 or H1299 cells transfected for 72 h either with control (Ctrl) or *Srsf2* siRNA in chromatin-enriched fractions (upper panels) and WCEs. Numbers represent the quantification of the densitometric signals according to histone H3 signal. $n = 3$. (**D**) Co-IP of SRSF2-HA or SRSF2(P95H)-HA with MRE11, RAD50, or NBS1 proteins in A549 cells transiently transfected for 24 h with pcDNA3.1 (Ctrl), pcDN3.1-SRSF2-HA, or pcDNA3.1-SRSF2(P95H)-HA plasmid. Input represents 10% of the immunoprecipitates. A representative experiment out of three is presented. (**E**) Biolayer interferometry using recombinant MRE11 as a bait and *in vitro* transcribed/translated pcDNA3.1 (lysate), SRSF2-HA (SRSF2), or SRSF2(P95H)-HA (SRSF2-P95H) plasmid. Upper panel: Western blotting of *in vitro* transcribed/translated recombinant proteins using anti-HA antibody. Ctrl: pcDNA3.1. (**F**) Upper panel: PLA for the detection of endogenous SRSF2 and MRE11 interaction in A549 cells. Ctrl – (negative control): PLA with mouse anti-SRSF2 antibody only. Scale bar = 10 μm. Lower panel: Quantification (mean ± SD) of the number of PLA spots/nucleus. $n = 3$ performed in duplicate (30–40 cells/condition). Mann–Whitney *t*-test, $^{**}P < .01$. (**G**) Representative immunoblots of indicated proteins in chromatin-enriched or RIPA extracts from A549 cells transiently transfected for 24 h with the indicated constructs. $n = 2$. (**H**) Upper panels: PLA for the detection of endogenous SRSF2 and MRE11 interaction in A549 cells treated or not (NT) with DRB (50 μM) for 6 h. Ctrl – (negative control): PLA with mouse anti-SRSF2 antibody only. SRSF2/MRE11: PLA with mouse anti-SRSF2 and rabbit anti-MRE11 antibodies. Scale bar = 10 μm. Lower panel: Quantification (mean ± SD) of the number of PLA spots/nucleus. $n = 3$ performed in duplicate (30–40 cells/condition). Mann–Whitney *t*-test, $^{**}P < .01$. In data, α-tubulin, and histone H3 were used as loading controls for whole cell and chromatin-enriched fractions, respectively.

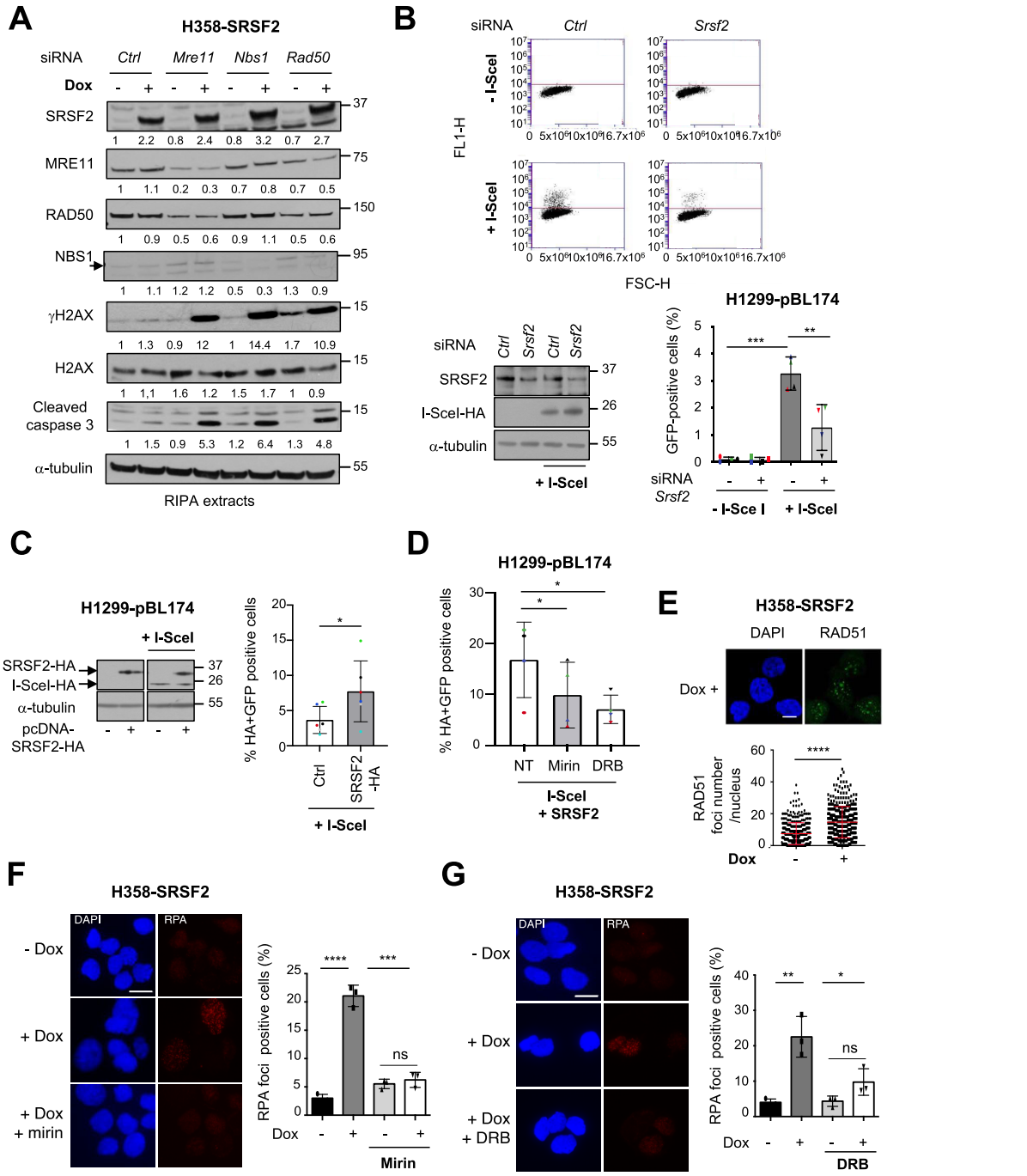


**Figure 5.** SRSF2 promotes DNA repair by HR. (**A**) H358-SRSF2 cells were transfected with mismatch (ctrl*)*, *mre11*, *nbs1*, or *rad50* siRNA for 48 h and treated (+) or not (−) with doxycycline (Dox) (1 μg/ml) for additional 24 h. Representative immunoblots of indicated proteins are shown. Numbers represent densitometric quantification of specific protein signal normalized to α-tubulin signal. $n = 3$. (B–D) Quantification of DSB-induced HR in H1299 clones stably expressing the pDR-GFP (pBL174) plasmid. When these cells are transfected with the pBL133 plasmid encoding the I-SceI restriction enzyme, efficient recombination restores a functional GFP-coding sequence. (**B**) Quantification of DSB-induced HR in H1299-pBL174 cells transfected with control (Ctrl) or *Srsf2* siRNAs and either pcDNA3.1 (−I-SceI) or pBL133 (+I-SceI). Upper panels: Representative FL1-H versus FSC-H dot plots of GFP-positive (FL1-H +) and –negative (FL1-H −) cells. Lower left panel: Western blotting of SRSF2 and I-SceI-HA. Lower right panel: Percentage of GFP-positive cells. $n = 4$. Unpaired *t*-test, $^{***}P < .001$, $^{**}P < .01$. (**C**) Quantification of DSB-induced HR in H1299-pBL174 cells co-transfected with pBL133 (+I-SceI) and either pcDNA3.1 (Ctrl) or pcDNA3.1-SRSF2-HA. Left panel: Western blotting of HA-tagged SRSF2 and I-SceI proteins. Right panel: Percentage of HA-/GFP-positive transfected cells determined by flow cytometry. $n = 6$. Paired *t*-test, $^{*}P < .05$. (**D**) Quantification of DSB-induced HR in H1299-pBL174 cells co-transfected with pBL133 (+I-SceI) together with pcDNA3.1-SRSF2-HA (SRSF2) and treated or not (NT) with mirin (40 μM) or DRB (50 μM). Percentage of HA-/GFP-positive transfected cells was determined by flow cytometry. $n = 4$. Paired *t*-test, $^{*}P < .05$. (**E**) H358-SRSF2 clones were cultured with (+) or without (−) doxycycline (Dox) (1 μg/ml) for 24 h. Upper panels: Representative images of RAD51 immunostaining. DAPI was used to counterstain nuclei. Scale bar = 10 μm. Lower panel: Quantification of the number of RAD51 foci/nucleus. Mean ± SD. $n = 3$. Mann–Whitney *t*-test, $^{****}P < .0001$. (**F**, **G**) H358-SRSF2 cells were cultured with (+) or without (−) doxycycline (Dox) (1 μg/ml) for 48 h in the presence or absence of mirin (40 μM, 24 h co-treatment, panel F) or DRB (50 μM, 6 h co-treatment, panel G). Left panels: Representative images of RPA IF. Scale bar = 20 μm. Right panels: Quantification (mean ± SD) of RPA-positive cells (%) in each condition. $n = 3$. Unpaired *t*-test, $^{****}P < .0001$, $^{***}P < .001$, $^{**}P < .01$, $^{*}P < .05$, ns: not significant. All data, α-Tubulin was used as a loading control.

suggesting that MRN serves to lower DSBs and prevent apoptosis when SRSF2 is overexpressed. MRE11 is a key protein regulating DNA repair in several contexts [66], and defective DNA repair could also account for increased DSBs in SRSF2-overexpressing cells. Therefore, to disentangle the contribution of SRSF2 together with MRE11 in DSB production and repair, we analyzed the effects of SRSF2 on the two main DSB repair pathways, HR and c-NHEJ. To study HR repair, we generated clones of H1299 LUAD cells stably expressing the pBL174-pDR-GFP plasmid (referred as H1299-pBL174 clones). This substrate allows the monitoring of HR repair of a DSB induced by the nuclease I-SceI through the recreation of a functional GFP (see the "Materials and methods" section). In these cells, siRNA-mediated depletion of endogenous SRSF2 decreased the percentage of GFP-positive cells in response to I-SceI expression (Fig. 5B). Conversely, overexpression of SRSF2 following transfection with a SRSF2-HA-encoding plasmid in H1299-pBL174 cells increased the percentage of GFP-positive cells (Fig. 5C). Such increase was prevented by inhibiting MRE11 exonuclease activity with mirin (Fig. 5D), consistent with the known function of MRE11 in resecting DNA to promote HR and DSB repair [63]. Overexpression of SRSF2 in H358 cells also resulted in an increased number of cells positive for the HR repair factors RAD51 (Fig. 5E) and RPA (Fig. 5F and G), and mirin prevented RPA foci formation in H358 cells overexpressing SRSF2 (Fig. 5F). In SRSF2-overexpressing cells, all RPA-positive cells were also γH2AX-positive but not all γH2AX-positive cells were RPA-positive. However, the percentage of RPA-positive cells among γH2AX-positive cells was increased upon SRSF2 induction as compared with control cells (Supplementary Fig. S6). Although the number of γH2AX-positive cells in control condition was low, this might be consistent with SRSF2 favoring HR. We also tested whether transcription could play a role in SRSF2-induced HR. As for mirin, DRB treatment decreased the percentage of GFP-positive H1299-pBL174 cells co-expressing SRSF2-HA and I-SceI-HA (Fig. 5D), and the number of RPA-positive cells in SRSF2-overexpressing H358 cells (Fig. 5G). Therefore, active transcription appears to be required for SRSF2-induced HR although we cannot fully exclude that the decreased number of RPA-positive cells detected upon DRB treatment in SRSF2-overexpressing cells somewhat reflects DRB inhibitory effects on DNA damage production (Fig. 3C and D).

Next, to analyze DSB repair by c-NHEJ, we established stable clones by transfecting A549 cells with the pBL230 plasmid that allows to monitor repair of I-SceI-induced DSBs by c-NHEJ through the expression of CD4 (see the "Materials and methods" section). In these clones, depletion of SRSF2 with siRNAs increased the percentage of CD4-positive cells (Fig. 6A and B). To investigate the mechanism underlying the inhibitory effect of SRSF2 on c-NHEJ, we analyzed the expression of a key c-NHEJ protein, 53BP1. In both A549 and H1299 cells, the knockdown of SRSF2 by siRNA increased 53BP1 protein level (Fig. 6C), while both immunoblotting (Fig. 6D) and IF microscopy (Fig. 6E) revealed a strong and significant decrease of 53BP1 protein levels in response to SRSF2 overexpression in H358 cells. This correlated with a slight decrease of *53BP1* mRNA levels as quantified by RT-qPCR (Fig. 6F). Mirin prevented the decreased expression of 53BP1 upon SRSF2 overexpression in H358 cells as detected by IF (Fig. 6G) and immunoblotting (Fig. 6H), suggesting that the exonuclease activity of MRE11 is required for SRSF2-induced 53BP1 down-regulation. Overall, our data reveal a role of SRSF2 in DSB repair, which involves MRE11, and which results in increased HR and decreased c-NHEJ in lung cancer cells. This suggests that accumulation of DNA damage in SRSF2-overexpressing cells may be caused by both increased DSB production following TRCs, as well as decreased repair by c-NHEJ. Although it does not fully compensate for the defective c-NHEJ, the SRSF2-mediated increase in HR, along with MRE11, likely maintains genomic instability below a level compatible with the survival of SRSF2-overexpressing cells.

## High levels of SRSF2 and MRE11 correlate with tumor progression in LUAD patients

We previously reported that SRSF2 is overexpressed in LUAD patients and that high levels of SRSF2 are associated with more advanced stages [27]. Given the direct cross talk between SRSF2 and MRE11 proteins and its functional relevance in lung cancer cells (Figs 4–6), we analyzed MRE11 expression by IHC in a series of 77 human NSCLCs, including 41 LUADs and 36 LUSC in which we had previously analyzed SRSF2 expression by IHC [27]. We showed that MRE11 was highly expressed in most of these tumors (Fig. 7A). We also found a positive correlation between MRE11 and SRSF2 IHC scores in tumors (Fig. 7B, $r = 0.2693$, $P = .0186$, Spearman). To go further, we took advantage of various publicly available transcriptomic cohorts of LUAD patients. In the TCGA LUAD cohort ($n = 524$ patients), we found that primary lung tumors displayed higher levels of *Srsf2* and *Mre11* mRNAs compared with normal lung tissues (Fig. 7C). We also found a positive correlation between *Srsf2* and *Mre11* mRNA levels in primary tumors but not in normal lung tissues (Fig. 7D upper panel, $r = 0.23$, $P < .0001$), which was consistent with our IHC results. Interestingly, an inverse relationship was also found between *Srsf2* and *53BP1* mRNA levels both in primary tumors (Fig. 7D lower panel, $r = -0.1944$, $P < .0001$) and normal lung tissues ($r = -0.2831$, $P = .0298$) which was consistent with our *in vitro* data in LUAD cells (Fig. 6F). These results regarding *Srsf2* and *Mre11* mRNA levels were confirmed using another database (GSE72094; $n = 442$ patients; Supplementary Fig. S7). More importantly, when clinico-pathological parameters were considered, we found that among early-stage LUAD patients from TCGA with high levels of *Srsf2* mRNA (up to the median, $n = 134$), those with the highest levels of *Mre11* mRNA (>75th percentile, $n = 45$) displayed the worse prognosis (Fig. 7E; $P = .0357$, log-rank test). Similar results were found by using another dataset (GSE68465; $n = 442$ patients; Supplementary Fig. S8). In this later cohort, among LUAD patients with high levels of *Srsf2* (up to the median, $n = 221$), those with the highest levels of *Mre11* mRNA (>75th percentile, 4th quartile, $n = 58$) exhibited a poorest prognosis whatever the stage ($P = .0213$, Gehan–Breslow–Wilcoxon test). Taken together, these results suggest that SRSF2 and MRE11 contribute together to LUAD progression.

## SRSF2 knockdown impacts late DSB repair in response to IR in LUAD cells

We finally wondered whether SRSF2 could also play a role in DSB repair in response to other DSB inducers. Hence, we previously reported that SRSF2 accumulates in response to cisplatin in H358 cells [30] and PLA experiments

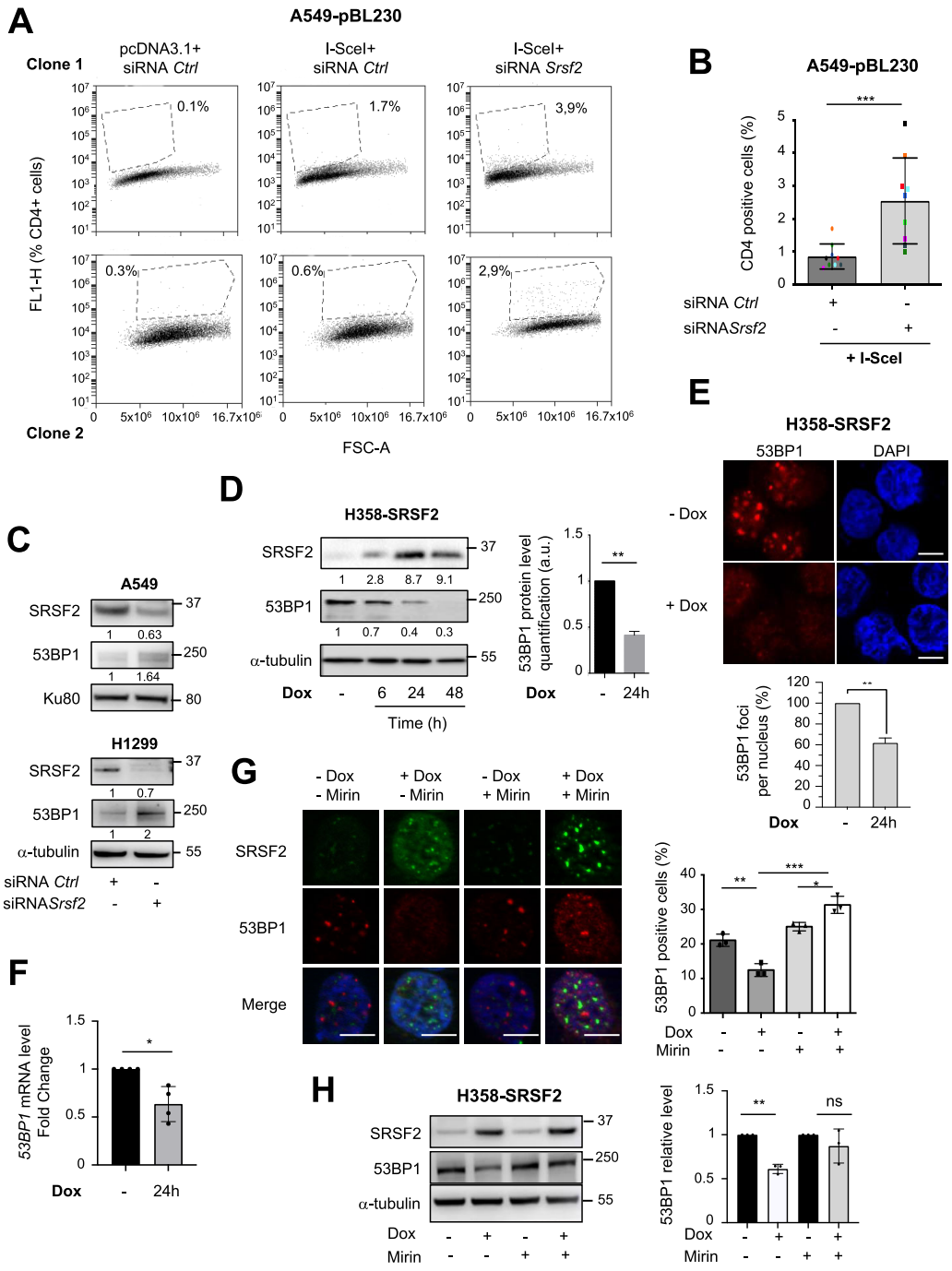


**Figure 6.** SRSF2 inhibits Nonhomologous End Joining (c-NHEJ) which correlates with down-regulation of 53BP1 protein level. (A, B) A549-pBL230 clones were transfected with control (Ctrl) or *Srsf2* siRNAs for 24 h and then transfected with pcDNA3.1 or pBL133 plasmid for 4 additional days. (**A**) Representative dot plots of CD4-positive transfected cells in two different clones using flow cytometry. (**B**) Percentage of CD4-positive recombinant cells in control or *Srsf2* knockdown cells. Mean ± SD. $n = 9$. Mann–Whitney *t*-test, $***P < .001$. (**C**) A549 or H1299 cells were transfected with *Ctrl* or *Srsf2* siRNA for 72 h. Representative immunoblots of indicated proteins in WCEs. $n = 3$. α-Tubulin or Ku80 was used as a loading control. Numbers represent densitometric quantification of specific protein signal normalized to α-tubulin or Ku80 signal. (**D**) Left panel: Representative immunoblots of indicated proteins in H358-SRSF2 cells cultured with or without doxycycline (1 μg/ml) for indicated times. α-Tubulin was used as a loading control. Right panel: Relative 53BP1/α-tubulin ratios are represented in comparison to the untreated condition which was arbitrarily assigned to 1. $n = 3$. Unpaired *t*-test, $**P < .01$. (E-H) H358-SRSF2-inducible cells were cultured or not for 24 h in the presence or absence of doxycycline (1 μg/ml). In some experiments, mirin (40 μM) was added. (**E**) Upper panel: Representative images of 53BP1 immunostaining. Scale bar = 10 μm. Lower panel: Quantification of 53BP1 foci/nucleus with values obtained in none-induced cells being arbitrarily assigned to 100%. Mean ± SD. $n = 3$. Unpaired *t*-test, $**P < .01$. (**F**) 53BP1 mRNA level (fold change ± SD compared with control). $n = 4$. Unpaired *t*-test, $*P < .05$. (G, H) H358-SRSF2 cells were cultured with (+) or without (–) doxycycline (Dox) (1 μg/ml) for 24 h and co-treated or not with mirin (40 μM) as indicated. (**G**) Left panels: Representative images of SRSF2 and 53BP1 immunostainings. DAPI was used to counterstain the nucleus. Scale bar = 10 μm. Right panel: Quantification (mean ± SD) of 53BP1-positive cells (%) defined as cells with >5 foci/nucleus. $n = 3$ (50–60 nuclei/condition/experiment). Unpaired *t*-test, $*p < .05$, $**p < .01$, $***p < .001$. (**H**) Left panels: Representative immunoblots of indicated proteins. α-Tubulin was used as a loading control. $n = 3$. Right panel: Relative level of 53BP1 protein according to α-tubulin signal. Values obtained in noninduced conditions were arbitrarily assigned to 1. Unpaired *t*-test, $**P < .01$, ns: not significant.

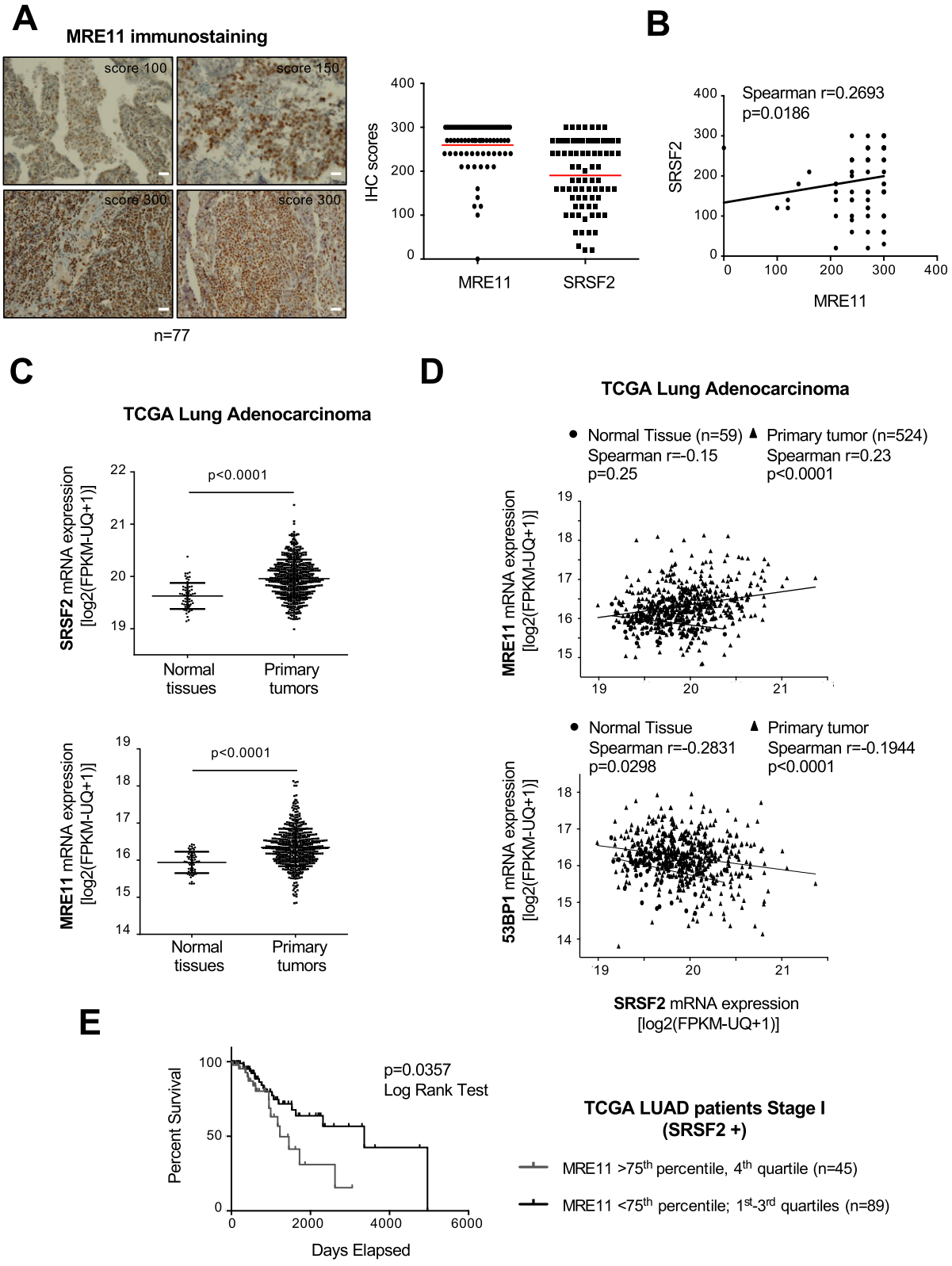


**Figure 7.** High level of both *Srsf2* and *Mre11* mRNAs correlates with poor prognosis in stage I LUAD patients. (**A**) Left panels: Representative MRE11 immunostainings from paraffin-embedded sections of LUAD patients. Immunoscores are indicated for each case. Right panel: Distribution of IHC scores of MRE11 and SRSF2 in NSCLC patients. (**B**) Spearman correlation between SRSF2 and MRE11 immunoscores. (**C**) Normalized *Srsf2* (upper panel) and *Mre11* (lower panel) mRNA levels [log2(FPKM-UQ + 1)] in LUAD patients and matched normal lung tissues retrieved from the TCGA ($n = 524$ for primary LUAD tumors and $n = 59$ for matched normal tissues) using UCSC Xena platform. *P*-values were calculated using an unpaired *t*-test. (**D**) Relationship between normalized *Srsf2* and *Mre11* (upper panel) or *53BP1* (lower panel) mRNA levels in normal lung tissues and LUAD patients. Spearman correlation. (**E**) Kaplan–Meier univariate survival analysis of early stage (pTNM I) LUAD patients from TCGA displaying high level of *Srsf2* mRNA (up to median, $n = 134$) and either high (>75th percentile, 4th quartile, $n = 45$) or low/medium (<75th percentile, 1st–3rd quartiles, $n = 89$) *Mre11* mRNA levels. Log-rank test.

demonstrated increased SRSF2/γH2AX and SRSF2/MRE11 closed proximity in response to cisplatin in A549 cells (Fig. 1F and Supplementary Fig. S4). IRs are strong and rapid inducers of DSBs. Interestingly, in H358 and A549 cells, SRSF2 protein levels tended to increase 24 h after IR, mainly at high doses (8–10 Gy) (Fig. 8A). To deepen the impact of SRSF2 on the repair of IR-induced DSBs, the kinetic of γH2AX foci formation and recovery was followed by IF at different timepoints (2, 4, 6, 24 h) after 3 Gy irradiation in A549 cells depleted or not of SRSF2 by siRNA. As compared with control cells, SRSF2-depleted cells retained a higher number of γH2AX nuclear foci 24 h after IR although no significant difference was observed at earlier timepoints (Fig. 8B). Similar results were obtained in another LUAD cell line, H1299 cells (Fig. 8C), as well as using another siRNA against *Srsf2* (Supplementary Fig. S9). These data indicate that the knockdown of SRSF2 delays late repair of DSBs induced by IR. Of note, in untransformed RPE cells, IR did not reproducibly increase SRSF2 protein level (Supplementary Fig. S10A) and the knockdown of SRSF2 by using two distinct siRNAs did not significantly impact clonogenic survival whatever the doses of IR (Supplementary Fig. S10B).

## Discussion

We have previously shown that the splicing factor SRSF2, a key member of SR protein family, is overexpressed in NSCLC and is associated with advanced stages in LUAD patients [27]. Deepening how altered SRSF2 expression impacts its functions is thus crucial to better understand the contribution of SRSF2 to tumor progression. Here, we provide molecular insights into the oncogenic functions of SRSF2. We report that SRSF2 overexpression in lung cancer cells leads to increased transcription, enhanced replicative stress, and accumulation of DNA damage, notably DSBs. We also provide evidence that SRSF2 regulates DNA repair by promoting HR while inhibiting c-NHEJ. At the molecular level, we highlight a closed interplay between SRSF2 and MRE11 or 53BP1 proteins. Coping with continued replicative stress and generation of DSBs, which contribute to mutations and chromosomal rearrangements [55], while maintaining a threshold of genomic instability compatible with survival represents an advantageous strategy for cancer progression. We propose that the fine control of DSB accumulation and repair by SRSF2, together with MRE11, is part of this strategy that allows lung cancer cell survival and thus promotes lung tumor progression (Fig. 9).

DNA damage induced by replication stress, in particular upon oncogene activation, is a fundamental step of tumorigenesis [67]. Replication fork slowing or stalling activates the replication stress response and the replication fork collapse can ultimately lead to DSB formation [10]. In this study, we showed that SRSF2 overexpression leads to replicative stress and replication-dependent DSBs, supporting oncogenic properties of SRSF2. A number of mechanisms can induce replication stress in response to oncogene activation, including deregulated replication initiation, increased reactive oxygen species, TRCs, altered nucleotide metabolism, or increased RNA synthesis [67]. This last mechanism, referred as "hypertranscription", has been described in response to activation of the oncogenes H-RAS$^{V12}$ and EWS–FLI1 or to estrogen-induced signaling [11, 52, 55, 68]. In this study, we showed that SRSF2 overexpression increases global transcription. Replicative SRSF2-overexpressing cells exhibited higher transcriptional increase compared with non-replicative cells. As we also showed that both replication and active transcription are required for SRSF2-induced DSBs, our results are consistent with TRCs inducing DNA damage in SRSF2-overexpressing cells. SRSF2 has been reported to play multiple roles in transcription, such as during elongation [48, 51], or release of paused RNA Polymerase II on active gene promoters where it collaborates with the noncoding RNA 7SK and promoter-associated nascent RNA [49]. Whether alteration of SRSF2 expression in our cells increases global RNA synthesis by impacting these processes remains to be deepened. R-loop formation is favored by increased RNA synthesis [52, 55]. We also provide evidence that SRSF2 overexpression in LUAD cells promotes R-loop accumulation. This was somewhat counterintuitive as previous studies have shown that inactivation of various components of the spliceosome machinery, including SR proteins, is associated with abnormal accumulation of R-loops [23, 56, 57]. Thus, these and our data suggest that SRSF2 protein level might be tightly controlled to prevent R-loop formation. Interestingly, R-loops also accumulate in response to SRSF2(P95H) mutation that frequently occurs in myelodysplastic syndromes and some leukemia but not in solid tumors [60]. R-loops can be either a source or a consequence of TRCs [69]. In SRSF2-overexpressing cells, we observed that γH2AX accumulation, DSBs, enhanced transcription, and slowing down of replication fork progression somewhat precede R-loop accumulation. Although the impact of R-loops in genomic instability in SRSF2-overexpressing cells remains to be deepened, these results suggest that they may not be the major source of DSBs in our cells, at least at early timepoints.

In addition to promoting DSBs, SRSF2 could favor DSBs accumulation by interfering with their repair. Some studies have already reported a link between the SR proteins SRSF1, SRSF3, or SRSF10 and DNA repair through the regulation of the expression/splicing of DNA repair factors, such as LIG-1, BRCA1, BRIP1, and RAD51 [70–73]. SRSF3 also promoted gemcitabine resistance in pancreatic cancer by enhancing DSB repair by HR through regulation of the splicing of lncRNA ANRIL [74]. Importantly, SRSF2 deficiency in primary human keratinocytes and oral squamous cell carcinoma was very recently found to cause DNA damage due to inefficient bidirectional transcription of DNA replication and repair genes, notably those involved in recombinational repair and DSB repair via HR [51]. In this study, we add further evidence that SRSF2 influences DSB repair by promoting HR in LUAD cell lines, which correlated with increased percentage of RPA- and RAD51-positive cells upon SRSF2 overexpression. Whether this is accompanied by enhanced transcription of HR repair genes remains to be determined. In addition, as we did not analyze in our cellular models the consequences of SRSF2 overexpression or knockdown on splicing changes, we cannot exclude that SRSF2-regulated splicing of genes involved in DNA repair or DDR might also contribute to some of the phenotypes we observed. We also provide additional results of a role of SRSF2 in inhibiting DSB repair by c-NHEJ, which is associated with decreased *53BP1* mRNA and protein levels. These data further support that a tight control of SRSF2 protein level might be required to regulate DNA repair, genomic stability, and cancer cell survival, as both SRSF2 knockdown and overexpression, which is often seen in solid tumors, are able to induce DNA damage. Furthermore, and supporting more enlarged functions of SRSF2 in DNA repair, we also

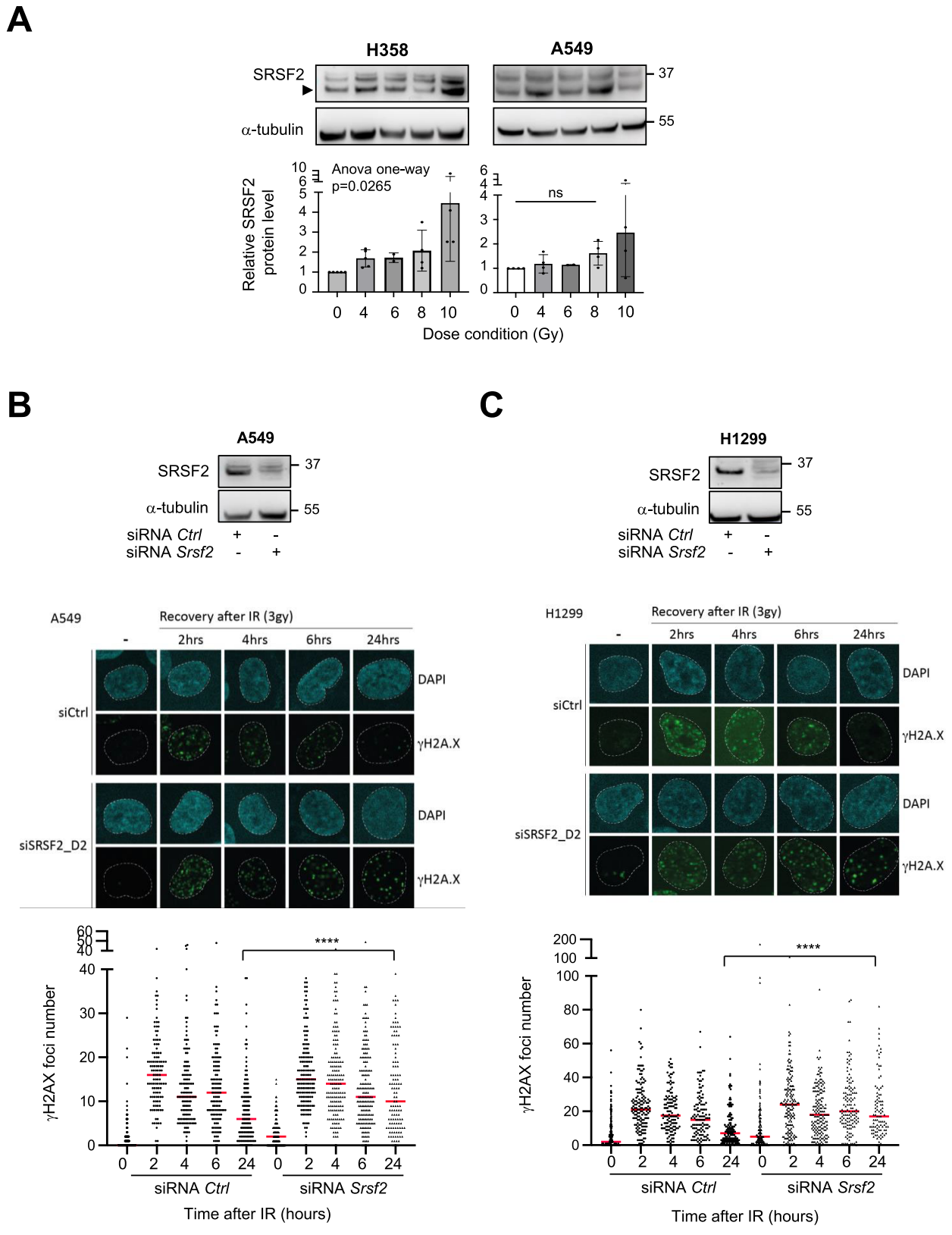


**Figure 8.** SRSF2 regulates DSB repair in response to IR in lung cancer cells. (**A**) H358 and A549 cells were irradiated at indicated doses. SRSF2 protein level was assessed by immunoblot in whole protein extracts 24 h after irradiation. Upper panels: Representative SRSF2 immunoblots. α-Tubulin was used as a loading control. Lower panels: SRSF2 relative level according to α-tubulin densitometric signal. Values obtained in nonirradiated cells were arbitrarily fixed to 1. $n = 4$. Anova one-way, ns: not significant. (**B**, **C**) A549 and H1299 cells were transfected with *Ctrl* siRNA or siRNA against SRSF2 for 72 h and submitted or not to 3 Gy irradiation. γH2AX nuclear foci were quantified at indicated times after recovery. Upper panels: SRSF2 representative immunoblots for knockdown efficiency. Middle panels: Representative immunostainings of γH2AX foci at indicated times after recovery. DAPI was used to counterstain the nucleus. Lower panels: Quantification of the number of γH2AX foci/nucleus in cells transfected with either *Ctrl* or *Srsf2* siRNA at indicated times. Median is indicated. $n = 3$. Unpaired *t*-test, $^{****}P < .0001$.

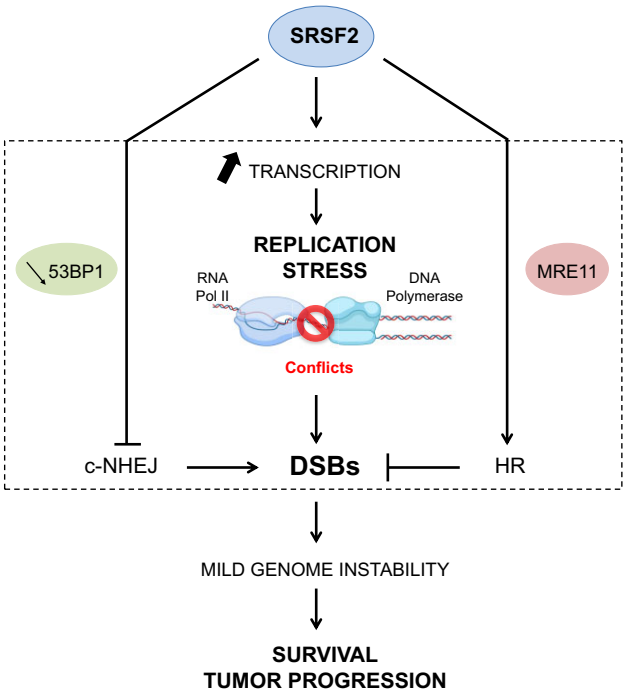


**Figure 9.** Model for SRSF2-induced lung tumor progression. High level of SRSF2 induces a global transcriptional increase in LUAD cells. This leads to enhanced replicative stress and DNA DSBs, likely as a result of conflicts between transcription and replication machineries. SRSF2 also controls DSB repair. SRSF2 inhibits c-NHEJ that correlates with a decrease of 53BP1 mRNA and protein levels. Conversely, a cross talk between SRSF2 and MRE11 proteins, which are both commonly increased in LUAD patients and are found in closed proximity in LUAD cells, increases DSB repair by HR. We propose that a high level of SRSF2, along with MRE11, tightly controls the balance between DSB production and repair helping to maintain genome instability below a threshold compatible with tumor cell survival, and thus, contributing to lung tumor progression.

provide evidence that SRSF2 knockdown in LUAD cells impacts the late repair of DSBs induced by IR. This suggest that SRSF2-deprived cells might be less prone to repair replication-associated DSBs that are secondary induced following IR and repaired by HR [75, 76].

Mechanistically, we unravel a strong interplay between SRSF2 and MRE11 proteins by showing that SRSF2 and MRE11 can directly interact *in vitro*, are in closed proximity in LUAD cells, and that SRSF2 regulates MRE11 recruitment to chromatin. MRE11 nuclease activity is required for SRSF2 functions in DNA repair as mirin prevents SRSF2-induced HR as a well as the decrease of the c-NHEJ protein 53BP1. Nonetheless, the role in DNA repair of the direct interaction between SRSF2 and MRE11 proteins remains to be elucidated further. We also showed that inhibiting RNA Polymerase II activity by using DRB decreases SRSF2/MRE11 PLA interactions in A549 cells, SRSF2-induced HR in H1299 pBL174 cells, as well as SRSF2-induced RPA foci accumulation. Although we cannot exclude that the negative effects of DRB in this last context somewhat reflect the decreased production of DSBs, our data support the idea that SRSF2, similar to H-RAS$^{V12}$ and EWS-FLI1, which enhance transcription and impact DSB repair pathways [77], could exert its oncogenic properties by interfering with DSB repair pathways and the recruitment of DNA repair components (e.g. MRE11) in response to enhanced TRCs.

We found that the knockdown of MRN with siRNA in SRSF2-overexpressing cells strongly enhances γH2AX accumulation and leads to apoptosis. More importantly, in LUAD patients, we found that MRE11 protein is highly expressed and that patients with high *Srsf2* and *Mre11* mRNA levels have the worse prognosis. Similar to other DNA repair proteins, MRE11 plays a pivotal role in preventing the deleterious effects of oncogene-induced replication stress [9, 10, 78–81]. By this way, MRE11 acts as a gatekeeper against tumor progression [82–84]. On the other hand, and supporting a more complex relationship between MRE11 expression and carcinogenesis, MRE11 is also highly expressed and predicts bad prognosis in breast cancers [85] or MYCN-amplified neuroblastoma in which MRE11 knockdown induces accumulation of replication stress and DNA damage biomarkers [86]. In addition, in a mouse model predisposed to spontaneous B-cell lymphomas, MRE11 promotes tumorigenesis by facilitating resistance to oncogene-induced replication stress [87]. Based on these previous studies and our data, we propose that MRE11 could attenuate TRCs induced by SRSF2 overexpression contributing, by this way, to the maintenance of genomic instability below a threshold compatible with the survival of SRSF2-overexpressing cells (Fig. 9).

In summary, we unravel a new oncogenic role of overexpressed SRSF2 involving both DSB production, as a result of increased transcription, enhanced replication-stress, and altered DNA repair, which may underlie lung tumor progression. Deciphering the molecular mechanisms controlling genome integrity in cancer cells may help providing new avenues for cancer treatment. Our data point towards the targeting of the SRSF2/MRE11 signaling node as a novel potential therapeutic strategy in NSCLC patients. In addition, as SRSF2 protein also accumulates in other cancer types, including breast, colon, ovarian, head and neck, glioblastoma and liver cancers compared with normal tissues [UALCAN database, [88]], it will be interesting to investigate further whether the consequences of SRSF2 overexpression detected in lung cancer might be relevant in other cancers.

## Acknowledgements

We thank the Microcell core facility of the Institute for Advanced Biosciences (UGA—Inserm U1209—CNRS 5309), especially Solenne Dufour, Jacques Mazzega, and Mylène Pezet, for their assistance with microscopes/confocal microscope (Jacques Mazzega) and flow cytometer (Mylène Pezet and Solenne Dufour), as well as Solenne Dufour for her help in quantifying BrdU incorporation experiments. This facility belongs to the IBISA-ISdV platform, member of the national infrastructure France-BioImaging supported by the French National Research Agency (ANR-10-INBS-04). We thank Dr Theo Ziegelmeyer and Mrs Perla Salameh for their help in quantifying γH2AX staining in some IF studies. Graphical abstract and Fig. 9 are created using BioRender.

*Author contributions*: All authors read and approved the final manuscript. Manal Khalife (Data curation, Formal analysis, Investigation, Methodology, Visualization), Tao Jia (Data curation, Formal analysis, Investigation, Methodology, Visualization, Writing—review & editing), Pierre Caron (Data curation, Formal analysis, Investigation, Methodology, Visualization, Writing—review & editing), Amani Shreim

(Data curation, Formal analysis, Investigation, Methodology, Visualization), Aurelie Genoux (Data curation, Investigation, Methodology), Agnese Cristini (Data curation, Formal analysis, Funding acquisition, Investigation, Methodology, Visualization, Writing—original draft, Writing—review & editing), Amelie Pucciarelli (Data curation, Investigation, Methodology), Marie Leverve (Investigation, Methodology), Nina Lepeltier (Investigation, Methodology), Néstor García-Rodríguez (Data curation, Formal analysis, Investigation, Methodology, Visualization, Writing—review & editing), Fabien Dalonneau (Data curation, Formal analysis, Investigation, Methodology), Shaliny Ramachandran (Data curation, Formal analysis, Investigation, Methodology, Visualization), Lara Fernandez Martinez (Investigation, Methodology), Guillaume Marcion (Data curation, Formal analysis, Investigation, Methodology, Visualization), Nicolas Lemaitre (Investigation, Methodology), Elisabeth Brambilla (Investigation, Methodology, Resources), Carmen Garrido (Investigation, Methodology, Writing—review & editing), Ester M. Hammond (Investigation, Methodology, Writing—review & editing), Pablo Huertas (Data curation, Formal analysis, Funding acquisition, Investigation, Methodology, Writing—review & editing), Sylvie Gazzeri (Data curation, Formal analysis, Investigation, Methodology, Visualization, Writing—review & editing), Olivier Sordet (Conceptualization, Data curation, Formal analysis, Funding acquisition, Investigation, Methodology, Validation, Visualization, Writing—original draft, Writing—review & editing), and Beatrice Eymin (Conceptualization, Data curation, Formal analysis, Funding acquisition, Investigation, Methodology, Project administration, Supervision, Validation, Visualization, Writing—original draft, Writing—review & editing)

## Supplementary data

Supplementary data is available at NAR Cancer online.

## Conflict of interest

None declared.

## Funding

This work was supported by Institut National de la Santé et de la Recherche Médicale (Inserm), by Centre National de la Recherche Scientifique (CNRS), by Univ. Grenoble Alpes, by the Fondation ARC (PJA 2014-1201788), by the Comités Départementaux Allier, Isère and Savoie de la Ligue Nationale contre le Cancer, by Institut National du Cancer (INCa) [INCa-PLBIO/Canceropole Ile de France (PLBIO-2014-08 to M.K., M.L., and A.P.); (INCA_16730 to P.C.)], by Région Auvergne-Rhône-Alpes (Programme Pack Ambition Recherche 2021), by Association Espoir Isère Contre Le Cancer, and by association GEFLUC Grenoble. T.J. was supported by INCa-PLBIO (INCa-PLBIO#2016-155). A.P. was funded by ERICAN program of Fondation MSDAVENIR (DS-2018-0015) supported by Canceropole CLARA. Work at Pablo Huertas' lab was funded by the R + D + I grant PID2019-104195G from the Spanish Ministry of Science and Innovation—Agencia Estatal de Investigación/10.13039/501100011033 and N.G.-R. was the recipient of a MSCA-IF-2017 (DNACHECK). CABIMER is supported by the regional government of Andalucia (Junta de Andalucía). O.S. lab is funded by the Inserm, the Institut National du Cancer (INCa) (INCA_16730 and INCA_19472), and the Fondation pour la Recherche Médicale (FRM) [Equipe labelisée FRM (DEQ20170839117)]. A.C. research is funded by Inserm, the Fondation ARC (Dossier n° ARCPJA2023090007177), and the Fondation de France (N° engagement: 00097702, 00113878, and 00119148). L.F.M. is supported by the La Ligue Nationale Contre le Cancer (IP/SC/SK-17250) and the Fondation pour la Recherche Médicale (Dossier n° FDT202404018232).

## Data availability

Flow cytometry data have been deposited in flow repository. Flow repository accession numbers are FR-FCM-Z8CG (Fig. 2A), FR-FCM-Z8CJ (Fig. 5B), FR-FCM-Z8CC (Fig. 5C), FR-FCM-Z8CD (Fig. 5D), FR-FCM-Z8CE (Fig. 6B), and FR-FCM-Z8CW (Supplementary Fig. S1B). Any additional information required to reanalyze the data reported in this paper is available upon request. The plasmids are available upon request.

## Consent for publications

All authors agree with the content of the manuscript.

## References

1. Pan Q, Shai O, Lee LJ *et al.* Deep surveying of alternative splicing complexity in the human transcriptome by high-throughput sequencing. *Nat Genet* 2008;**40**:1413–5. https://doi.org/10.1038/ng.259
2. Bradley RK, Anczukow O. RNA splicing dysregulation and the hallmarks of cancer. *Nat Rev Cancer* 2023;**23**:135–55. https://doi.org/10.1038/s41568-022-00541-7
3. Anczukow O, Allain FH, Angarola BL *et al.* Steering research on mRNA splicing in cancer towards clinical translation. *Nat Rev Cancer* 2024;**24**:887–905. https://doi.org/10.1038/s41568-024-00750-2
4. Zhang Q, Ai Y, Abdel-Wahab O. Molecular impact of mutations in RNA splicing factors in cancer. *Mol Cell* 2024;**84**:3667–80. https://doi.org/10.1016/j.molcel.2024.07.019
5. Urbanski LM, Leclair N, Anczukow O. Alternative-splicing defects in cancer: splicing regulators and their downstream targets, guiding the way to novel cancer therapeutics. *WIREs RNA* 2018;**9**:e1476. https://doi.org/10.1002/wrna.1476
6. Aguilera A, Garcia-Muse T. Causes of genome instability. *Annu Rev Genet* 2013;**47**:1–32. https://doi.org/10.1146/annurev-genet-111212-133232
7. Garcia-Muse T, Aguilera A. Transcription–replication conflicts: how they occur and how they are resolved. *Nat Rev Mol Cell Biol* 2016;**17**:553–63. https://doi.org/10.1038/nrm.2016.88
8. Saponaro M. Transcription–replication coordination. *Life (Basel)* 2022;**12**:108–16.
9. Hills SA, Diffley JF. DNA replication and oncogene-induced replicative stress. *Curr Biol* 2014;**24**:R435–44. https://doi.org/10.1016/j.cub.2014.04.012
10. Mazouzi A, Velimezi G, Loizou JI. DNA replication stress: causes, resolution and disease. *Exp Cell Res* 2014;**329**:85–93. https://doi.org/10.1016/j.yexcr.2014.09.030
11. Bowry A, Kelly RDW, Petermann E. Hypertranscription and replication stress in cancer. *Trends Cancer* 2021;**7**:863–77. https://doi.org/10.1016/j.trecan.2021.04.006
12. Bartkova J, Horejsi Z, Koed K *et al.* DNA damage response as a candidate anti-cancer barrier in early human tumorigenesis. *Nature* 2005;**434**:864–70. https://doi.org/10.1038/nature03482

13. Gorgoulis VG, Vassiliou LV, Karakaidos P *et al.* Activation of the DNA damage checkpoint and genomic instability in human precancerous lesions. *Nature* 2005;**434**:907–13. https://doi.org/10.1038/nature03485
14. Wickramasinghe VO, Venkitaraman AR. RNA processing and genome stability: cause and consequence. *Mol Cell* 2016;**61**:496–505. https://doi.org/10.1016/j.molcel.2016.02.001
15. Mikolaskova B, Jurcik M, Cipakova I *et al.* Maintenance of genome stability: the unifying role of interconnections between the DNA damage response and RNA-processing pathways. *Curr Genet* 2018;**64**:971–83. https://doi.org/10.1007/s00294-018-0819-7
16. Savage KI, Gorski JJ, Barros EM *et al.* Identification of a BRCA1–mRNA splicing complex required for efficient DNA repair and maintenance of genomic stability. *Mol Cell* 2014;**54**:445–59. https://doi.org/10.1016/j.molcel.2014.03.021
17. Adamson B, Smogorzewska A, Sigoillot FD *et al.* A genome-wide homologous recombination screen identifies the RNA-binding protein RBMX as a component of the DNA-damage response. *Nat Cell Biol* 2012;**14**:318–28. https://doi.org/10.1038/ncb2426
18. Polo SE, Blackford AN, Chapman JR *et al.* Regulation of DNA-end resection by hnRNPU-like proteins promotes DNA double-strand break signaling and repair. *Mol Cell* 2012;**45**:505–16. https://doi.org/10.1016/j.molcel.2011.12.035
19. Wang WY, Pan L, Su SC *et al.* Interaction of FUS and HDAC1 regulates DNA damage response and repair in neurons. *Nat Neurosci* 2013;**16**:1383–91. https://doi.org/10.1038/nn.3514
20. Marechal A, Li JM, Ji XY *et al.* PRP19 transforms into a sensor of RPA-ssDNA after DNA damage and drives ATR activation via a ubiquitin-mediated circuitry. *Mol Cell* 2014;**53**:235–46. https://doi.org/10.1016/j.molcel.2013.11.002
21. Tresini M, Warmerdam DO, Kolovos P *et al.* The core spliceosome as target and effector of non-canonical ATM signalling. *Nature* 2015;**523**:53–8. https://doi.org/10.1038/nature14512
22. Huertas P, Aguilera A. Cotranscriptionally formed DNA:RNA hybrids mediate transcription elongation impairment and transcription-associated recombination. *Mol Cell* 2003;**12**:711–21. https://doi.org/10.1016/j.molcel.2003.08.010
23. Li X, Manley JL. Inactivation of the SR protein splicing factor ASF/SF2 results in genomic instability. *Cell* 2005;**122**:365–78. https://doi.org/10.1016/j.cell.2005.06.008
24. Hamperl S, Cimprich KA. The contribution of co-transcriptional RNA:DNA hybrid structures to DNA damage and genome instability. *DNA Repair (Amst)* 2014;**19**:84–94. https://doi.org/10.1016/j.dnarep.2014.03.023
25. Jimenez M, Urtasun R, Elizalde M *et al.* Splicing events in the control of genome integrity: role of SLU7 and truncated SRSF3 proteins. *Nucleic Acids Res* 2019;**47**:3450–66. https://doi.org/10.1093/nar/gkz014
26. Zhou Z, Fu XD. Regulation of splicing by SR proteins and SR protein-specific kinases. *Chromosoma* 2013;**122**:191–207. https://doi.org/10.1007/s00412-013-0407-z
27. Gout S, Brambilla E, Boudria A *et al.* Abnormal expression of the pre-mRNA splicing regulators SRSF1, SRSF2, SRPK1 and SRPK2 in non small cell lung carcinoma. *PLoS One* 2012;**7**:e46539. https://doi.org/10.1371/journal.pone.0046539
28. Edmond V, Merdzhanova G, Gout S *et al.* A new function of the splicing factor SRSF2 in the control of E2F1-mediated cell cycle progression in neuroendocrine lung tumors. *Cell Cycle* 2013;**12**:1267–78. https://doi.org/10.4161/cc.24363
29. Merdzhanova G, Edmond V, De Seranno S *et al.* E2F1 controls alternative splicing pattern of genes involved in apoptosis through upregulation of the splicing factor SC35. *Cell Death Differ* 2008;**15**:1815–23. https://doi.org/10.1038/cdd.2008.135
30. Edmond V, Moysan E, Khochbin S *et al.* Acetylation and phosphorylation of SRSF2 control cell fate decision in response to cisplatin. *EMBO J* 2011;**30**:510–23. https://doi.org/10.1038/emboj.2010.333
31. Travis WD, Brambilla E, Noguchi M *et al.* International association for the study of lung cancer/American thoracic society/European respiratory society international multidisciplinary classification of lung adenocarcinoma. *J Thorac Oncol* 2011;**6**:244–85. https://doi.org/10.1097/JTO.0b013e318206a221
32. Foskolou IP, Biasoli D, Olcina MM *et al.* Measuring DNA replication in hypoxic conditions. *Adv Exp Med Biol* 2016;**899**:11–25. https://doi.org/10.1007/978-3-319-26666-4_2
33. Renaud E, Barascu A, Rosselli F. Impaired TIP60-mediated H4K16 acetylation accounts for the aberrant chromatin accumulation of 53BP1 and RAP80 in Fanconi anemia pathway-deficient cells. *Nucleic Acids Res* 2016;**44**:648–56. https://doi.org/10.1093/nar/gkv1019
34. Dungrawala H, Cortez D. Purification of proteins on newly synthesized DNA using iPOND. *Methods Mol Biol* 2015;**1228**:123–31. https://doi.org/10.1007/978-1-4939-1680-1_10
35. Cristini A, Ricci G, Britton S *et al.* Dual processing of R-loops and topoisomerase I induces transcription-dependent DNA double-strand breaks. *Cell Rep* 2019;**28**:3167–81. https://doi.org/10.1016/j.celrep.2019.08.041
36. Geraud M, Cristini A, Salimbeni S *et al.* TDP1 mutation causing SCAN1 neurodegenerative syndrome hampers the repair of transcriptional DNA double-strand breaks. *Cell Rep* 2024;**43**:114214. https://doi.org/10.1016/j.celrep.2024.114214
37. Marcion G, NF H.F., Uyanik B *et al.* Nanofitins targeting heat shock protein 110: an innovative immunotherapeutic modality in cancer. *Int J Cancer* 2021;**148**:3019–31. https://doi.org/10.1002/ijc.33485
38. Gozzi GJ, BC G.D., Dias AMM *et al.* Selecting the first chemical molecule inhibitor of HSP110 for colorectal cancer therapy. *Cell Death Differ* 2020;**27**:117–29. https://doi.org/10.1038/s41418-019-0343-4
39. Goldman MJ, Craft B, Hastie M *et al.* Visualizing and interpreting cancer genomics data via the Xena platform. *Nat Biotechnol* 2020;**38**:675–678. https://doi.org/10.1038/s41587-020-0546-8
40. Kabbout M, Garcia MM, Fujimoto J *et al.* ETS2 mediated tumor suppressive function and MET oncogene inhibition in human non-small cell lung cancer. *Clin Cancer Res* 2013;**19**:3383–95. https://doi.org/10.1158/1078-0432.CCR-13-0341
41. Director's Challenge Consortium for the Molecular Classification of Lung Adenocarcinoma, Shedden K, Taylor JMG *et al.* Gene expression-based survival prediction in lung adenocarcinoma: a multi-site, blinded validation study. *Nat Med* 2008;**14**:822–7. https://doi.org/10.1038/nm.1790
42. Schabath MB, Welsh EA, Fulp WJ *et al.* Differential association of STK11 and TP53 with KRAS mutation-associated gene expression, proliferation and immune surveillance in lung adenocarcinoma. *Oncogene* 2016;**35**:3209–16. https://doi.org/10.1038/onc.2015.375
43. Barrett T, Wilhite SE, Ledoux P *et al.* NCBI GEO: archive for functional genomics data sets–update. *Nucleic Acids Res* 2013;**41**:D991–5. https://doi.org/10.1093/nar/gks1193
44. Bonner WM, Redon CE, Dickey JS *et al.* GammaH2AX and cancer. *Nat Rev Cancer* 2008;**8**:957–67. https://doi.org/10.1038/nrc2523
45. Zeman MK, Cimprich KA. Causes and consequences of replication stress. *Nat Cell Biol* 2014;**16**:2–9. https://doi.org/10.1038/ncb2897
46. Sirbu BM, McDonald WH, Dungrawala H *et al.* Identification of proteins at active, stalled, and collapsed replication forks using isolation of proteins on nascent DNA (iPOND) coupled with mass spectrometry. *J Biol Chem* 2013;**288**:31458–67. https://doi.org/10.1074/jbc.M113.511337
47. Martinez de Duenas E, Gavila-Gregori J, Olmos-Anton S *et al.* Preclinical and clinical development of palbociclib and future perspectives. *Clin Transl Oncol* 2018;**20**:1136–44. https://doi.org/10.1007/s12094-018-1850-3

48. Lin S, Coutinho-Mansfield G, Wang D *et al.* The splicing factor SC35 has an active role in transcriptional elongation. *Nat Struct Mol Biol* 2008;**15**:819–26. https://doi.org/10.1038/nsmb.1461
49. Ji X, Zhou Y, Pandit S *et al.* SR proteins collaborate with 7SK and promoter-associated nascent RNA to release paused polymerase. *Cell* 2013;**153**:855–68. https://doi.org/10.1016/j.cell.2013.04.028
50. Mo S, Ji X, Fu XD. Unique role of SRSF2 in transcription activation and diverse functions of the SR and hnRNP proteins in gene expression regulation. *Transcription* 2013;**4**:251–9. https://doi.org/10.4161/trns.26932
51. Wagner RE, Arnetzl L, Britto-Borges T *et al.* SRSF2 safeguards efficient transcription of DNA damage and repair genes. *Cell Rep* 2024;**43**:114869. https://doi.org/10.1016/j.celrep.2024.114869
52. Kotsantis P, Silva LM, Irmscher S *et al.* Increased global transcription activity as a mechanism of replication stress in cancer. *Nat Commun* 2016;**7**:13087. https://doi.org/10.1038/ncomms13087
53. Hamperl S, Bocek MJ, Saldivar JC *et al.* Transcription–replication conflict orientation modulates R-loop levels and activates distinct DNA damage responses. *Cell* 2017;**170**:774–86. https://doi.org/10.1016/j.cell.2017.07.043
54. Gomez-Gonzalez B, Aguilera A. Transcription-mediated replication hindrance: a major driver of genome instability. *Genes Dev.* 2019;**33**:1008–26. https://doi.org/10.1101/gad.324517.119
55. Stork CT, Bocek M, Crossley MP *et al.* Co-transcriptional R-loops are the main cause of estrogen-induced DNA damage. *eLife* 2016;**5**:e17548. https://doi.org/10.7554/eLife.17548
56. Nguyen HD, Leong WY, Li W *et al.* Spliceosome mutations induce R loop-associated sensitivity to ATR inhibition in myelodysplastic syndromes. *Cancer Res* 2018;**78**:5363–74. https://doi.org/10.1158/0008-5472.CAN-17-3970
57. Singh S, Ahmed D, Dolatshad H *et al.* SF3B1 mutations induce R-loop accumulation and DNA damage in MDS and leukemia cells with therapeutic implications. *Leukemia* 2020;**34**:2525–30. https://doi.org/10.1038/s41375-020-0753-9
58. Paull TT. Mechanisms of ATM activation. *Annu Rev Biochem* 2015;**84**:711–38. https://doi.org/10.1146/annurev-biochem-060614-034335
59. Hartlerode AJ, Morgan MJ, Wu Y *et al.* Recruitment and activation of the ATM kinase in the absence of DNA-damage sensors. *Nat Struct Mol Biol* 2015;**22**:736–43. https://doi.org/10.1038/nsmb.3072
60. Chen L, Chen JY, Huang YJ *et al.* The augmented R-loop is a unifying mechanism for myelodysplastic syndromes induced by high-risk splicing factor mutations. *Mol Cell* 2018;**69**:412–25. https://doi.org/10.1016/j.molcel.2017.12.029
61. Kim E, Ilagan JO, Liang Y *et al.* SRSF2 Mutations contribute to myelodysplasia by mutant-specific effects on exon recognition. *Cancer Cell* 2015;**27**:617–30. https://doi.org/10.1016/j.ccell.2015.04.006
62. Paull TT, Deshpande RA. The Mre11/Rad50/Nbs1 complex: recent insights into catalytic activities and ATP-driven conformational changes. *Exp Cell Res* 2014;**329**:139–47. https://doi.org/10.1016/j.yexcr.2014.07.007
63. Syed A, Tainer JA. The MRE11-RAD50-NBS1 complex conducts the orchestration of damage signaling and outcomes to stress in DNA replication and repair. *Annu Rev Biochem* 2018;**87**:263–94. https://doi.org/10.1146/annurev-biochem-062917-012415
64. Dupre A, Boyer-Chatenet L, Sattler RM *et al.* A forward chemical genetic screen reveals an inhibitor of the Mre11–Rad50–Nbs1 complex. *Nat Chem Biol* 2008;**4**:119–25. https://doi.org/10.1038/nchembio.63
65. Shibata A, Moiani D, Arvai AS *et al.* DNA double-strand break repair pathway choice is directed by distinct MRE11 nuclease activities. *Mol Cell* 2014;**53**:7–18. https://doi.org/10.1016/j.molcel.2013.11.003
66. Stracker TH, Petrini JH. The MRE11 complex: starting from the ends. *Nat Rev Mol Cell Biol* 2011;**12**:90–103. https://doi.org/10.1038/nrm3047
67. Kotsantis P, Petermann E, Boulton SJ. Mechanisms of oncogene-induced replication stress: jigsaw falling into place. *Cancer Discov* 2018;**8**:537–55. https://doi.org/10.1158/2159-8290.CD-17-1461
68. Gorthi A, Romero JC, Loranc E *et al.* EWS-FLI1 increases transcription to cause R-loops and block BRCA1 repair in Ewing sarcoma. *Nature* 2018;**555**:387–91. https://doi.org/10.1038/nature25748
69. Stratigi K, Siametis A, Garinis GA. Looping forward: exploring R-loop processing and therapeutic potential. *FEBS Lett* 2025;**599**:244–66.
70. He X, Zhang P. Serine/arginine-rich splicing factor 3 (SRSF3) regulates homologous recombination-mediated DNA repair. *Mol Cancer* 2015;**14**:158. https://doi.org/10.1186/s12943-015-0422-1
71. Shkreta L, Toutant J, Durand M *et al.* SRSF10 connects DNA damage to the alternative splicing of transcripts encoding apoptosis, cell-cycle control, and DNA repair factors. *Cell Rep* 2016;**17**:1990–2003. https://doi.org/10.1016/j.celrep.2016.10.071
72. Martinez-Terroba E, Ezponda T, Bertolo C *et al.* The oncogenic RNA-binding protein SRSF1 regulates LIG1 in non-small cell lung cancer. *Lab Invest* 2018;**98**:1562–74. https://doi.org/10.1038/s41374-018-0128-2
73. Lin W, Xu L, Li Y *et al.* Aberrant FAM135B attenuates the efficacy of chemotherapy in colorectal cancer by modulating SRSF1-mediated alternative splicing. *Oncogene* 2024;**43**:3532–44. https://doi.org/10.1038/s41388-024-03189-9
74. Wang ZW, HJF P.J., Zhang JQ *et al.* SRSF3-mediated regulation of N6-methyladenosine modification-related lncRNA ANRIL splicing promotes resistance of pancreatic cancer to gemcitabine. *Cell Rep* 2022;**39**:3532–44. https://doi.org/10.1016/j.celrep.2022.110813
75. Groth P, Orta ML, Elvers I *et al.* Homologous recombination repairs secondary replication induced DNA double-strand breaks after ionizing radiation. *Nucleic Acids Res* 2012;**40**:6585–94. https://doi.org/10.1093/nar/gks315
76. Nickoloff JA, Sharma N, Allen CP *et al.* Roles of homologous recombination in response to ionizing radiation-induced DNA damage. *Int J Radiat Biol* 2023;**99**:903–14. https://doi.org/10.1080/09553002.2021.1956001
77. Tu Z, Aird KM, Bitler BG *et al.* Oncogenic RAS regulates BRIP1 expression to induce dissociation of BRCA1 from chromatin, inhibit DNA repair, and promote senescence. *Dev Cell* 2011;**21**:1077–91. https://doi.org/10.1016/j.devcel.2011.10.010
78. Bryant HE, Petermann E, Schultz N *et al.* PARP is activated at stalled forks to mediate Mre11-dependent replication restart and recombination. *EMBO J* 2009;**28**:2601–15. https://doi.org/10.1038/emboj.2009.206
79. Trenz K, Smith E, Smith S *et al.* ATM and ATR promote Mre11 dependent restart of collapsed replication forks and prevent accumulation of DNA breaks. *EMBO J* 2006;**25**:1764–74. https://doi.org/10.1038/sj.emboj.7601045
80. Schlacher K, Christ N, Siaud N *et al.* Double-strand break repair-independent role for BRCA2 in blocking stalled replication fork degradation by MRE11. *Cell* 2011;**145**:529–42. https://doi.org/10.1016/j.cell.2011.03.041
81. Ying S, Hamdy FC, Helleday T. Mre11-dependent degradation of stalled DNA replication forks is prevented by BRCA2 and PARP1. *Cancer Res* 2012;**72**:2814–21. https://doi.org/10.1158/0008-5472.CAN-11-3417
82. Bender CF, Sikes ML, Sullivan R *et al.* Cancer predisposition and hematopoietic failure in Rad50(S/S) mice. *Genes Dev* 2002;**16**:2237–51. https://doi.org/10.1101/gad.1007902
83. Dumon-Jones V, Frappart PO, Tong WM *et al.* Nbn heterozygosity renders mice susceptible to tumor formation and ionizing radiation-induced tumorigenesis. *Cancer Res* 2003;**63**:7263–9.
84. Gupta GP, Vanness K, Barlas A *et al.* The Mre11 complex suppresses oncogene-driven breast tumorigenesis and metastasis. *Mol Cell* 2013;**52**:353–65. https://doi.org/10.1016/j.molcel.2013.09.001

85. Yuan SS, Hou MF, Hsieh YC *et al.* Role of MRE11 in cell proliferation, tumor invasion, and DNA repair in breast cancer. *J Natl Cancer Inst* 2012;**104**:1485–502. https://doi.org/10.1093/jnci/djs355
86. Petroni M, Sardina F, Infante P *et al.* MRE11 inhibition highlights a replication stress-dependent vulnerability of MYCN-driven tumors. *Cell Death Dis* 2018;**9**:895. https://doi.org/10.1038/s41419-018-0924-z
87. Spehalski E, Capper KM, Smith CJ *et al.* MRE11 promotes tumorigenesis by facilitating resistance to oncogene-induced replication stress. *Cancer Res* 2017;**77**:5327–38. https://doi.org/10.1158/0008-5472.CAN-17-1355
88. Chandrashekar DS, Karthikeyan SK, Korla PK *et al.* UALCAN: an update to the integrated cancer data analysis platform. *Neoplasia* 2022;**25**:18–27. https://doi.org/10.1016/j.neo.2022.01.001

**Received:** February 24, 2023. **Revised:** February 4, 2025. **Editorial Decision:** March 10, 2025. **Accepted:** March 13, 2025